

1 **A special envelope separates extra-chromosomal from
2 mammalian chromosomal DNA in the cytoplasm**

3

4 Laura Schenkel, Xuan Wang, Nhung Le⁺, Michael Burger and Ruth Kroschewski

5 *ETH Zürich, Institute of Biochemistry, Otto-Stern-Weg 3, 8093 Zürich, Switzerland*

6

7 ⁺ current address:

8 VNU University of Science, 334 Nguyen Trai street, Thanh Xuan district, Hanoi city, Vietnam.

9

10 **Abstract**

11 Expression from transfected plasmid DNA is generally transient, but little do we know on what
12 limits this. Live-cell imaging revealed that DNA transfected into mammalian cells was either
13 captured directly in the cytoplasm, or was soon expelled from the nucleus, upon its entry. In
14 the cytoplasm, plasmid DNA was rapidly surrounded by a double membrane and frequently
15 colocalized with extra-chromosomal DNA of telomeric origin, also expelled from the nucleus.
16 Therefore, we termed this long-term maintained structure exclusome. The exclusome
17 envelope contains endoplasmic reticulum proteins, the inner-nuclear membrane proteins
18 Lap2 β and Emerin but differs from the nuclear envelope by the absence of the Lamin B
19 Receptor, nuclear pore complexes and by the presence of fenestrations. Further, Emerin
20 affects the frequency of cells with exclusomes. Thus, cells wrap chromosomes and extra-
21 chromosomal DNA into similar yet distinct envelopes. Thereby, they distinguish, sort, cluster,
22 package, and keep extra-chromosomal DNA in the exclusome but chromosomal DNA in the
23 nucleus, where transcription occurs.

24

25 **Running title:** The exclusome tells plasmid DNA from chromosomes

26

27 **Introduction**

28

29 In all eukaryotes the genome is enclosed in the nucleus, which compartmentalizes the
30 chromosomes away from the cytoplasm (Güttinger et al., 2009). The separation between
31 nucleoplasm and cytoplasm is ensured by a flat double membrane derived from the
32 endoplasmic reticulum (ER). Exchange between the nucleoplasm and the cytoplasm occurs
33 mainly through pores in this double membrane which are made selective by nuclear pore
34 complexes (NPCs). Such NPC-containing double membrane is further specialized, e.g., by
35 the presence of inner-nuclear membrane (INM) proteins, constituting the nuclear envelope. In
36 many species, the nuclear envelope breaks down in mitosis and reassembles around the
37 chromosomes upon mitotic exit. Whether nuclear envelope assembly is somehow restricted
38 to chromosomes at the end of mitosis or if it can take place around any DNA in the cytoplasm
39 and even throughout the cell cycle is unknown.

40

41 How mammalian cells assemble the nuclear envelope at the end of mitosis has been
42 intensively studied. When the separated chromosomes are pulled to opposite spindle poles
43 towards the end of anaphase, tubular ER membranes approach each segregating
44 chromosomal mass from several sides establishing the beginnings of two nuclear envelopes
45 (Anderson and Hetzer, 2007; Anderson and Hetzer, 2008). But still the trigger for membranes,
46 being not necessarily exclusively ER, to approach and then contact the separated
47 chromosomes is unresolved (Kutay et al., 2021; Schellhaus et al., 2016). Barrier-to-
48 autointegration factor (BAF, BANF), which sequence unspecifically binds DNA, accumulates
49 at the surface of mitotic chromosomes (Samwer et al., 2017; Zheng et al., 2000). BAF is
50 required for wrapping the chromosomes in membranes, which contain initially several
51 homogeneously distributed transmembrane proteins of the LAP2, Emerin, MAN1 (LEM)-
52 domain family (Haraguchi et al., 2000; Haraguchi et al., 2001; Kobayashi et al., 2015). BAF
53 binds to the LEM-domain of e.g., Emerin, and thereby establishes a DNA membrane tether
54 (Lee et al., 2001). NPC assembly occurs after membrane patches established contact with
55 the chromosomes and contribute to nuclear envelope sealing (Kutay et al., 2021; Otsuka et
56 al., 2018). Would these events indistinctively take place and wrap up any type of DNA or are
57 they exclusive to chromosomes?

58

59 In addition to the special case of mitochondria, there are situations *in vivo* where DNA is
60 enwrapped by a membrane. For example, late in anaphase, lagging chromosomes can be
61 enwrapped in an envelope and thus separate from the main nucleus, forming structures called
62 micronuclei. Initially, the micronuclear envelope has all the characteristics of a nuclear
63 envelope (Hatch et al., 2013). However, it degenerates over time. Over this period the

64 enclosed DNA becomes fragmented and during one of the following mitoses the fragments
65 reintegrate into chromosomes (Crasta et al., 2012; Zhang et al., 2015). In micronuclei, loss of
66 Lamin B1 correlates with their decay (Hatch et al., 2013). It is not known, however, what makes
67 micronuclei degenerate while the nucleus stays intact. Remarkably, lagging chromosomes
68 were shown to be frequent. Yet, they were transient, hardly forming micronuclei, as they
69 mostly reintegrated during the mitosis in which they appeared into the reforming nucleus in
70 human non-transformed and transformed cell lines (Orr et al., 2021). Also in *Drosophila*
71 *melanogaster* neuronal stem cells, chromatin fragments originating from chromosome ends
72 were rarely found in micronuclei (Karg et al., 2015). Instead, these fragments either rejoined
73 early in anaphase a membrane-free chromosomal mass or they rejoined newly formed nuclei
74 via nuclear envelope channels and by tethering to chromosome ends later in anaphase (Karg
75 et al., 2015; Warecki et al., 2020). Thus, lagging chromosomes mostly rejoin nuclei within the
76 same mitosis or they form less frequently unstable micronuclei, where the fragmented
77 micronuclear DNA ends up in nuclear chromosomes after some divisions. Remarkably,
78 syncytia, which are cells with multiple stable nuclei, exist. All these nuclei are roughly of similar
79 size as seen in the slime mold *Physarum polycephalum* and human osteoclasts (Gerber et al.,
80 2022; Kopesky et al., 2014). In contrast micronuclei in mammalian cells are at least 5 times
81 smaller than their corresponding nuclei (Kneissig et al., 2019). Therefore, separate nuclei and
82 nucleus-like structures can form in the same cell but in many instances the smaller structures
83 are unstable.

84
85 Remarkably, circular extra-chromosomal DNA excised from chromosomes, thus of
86 endogenous origin, exists in every cell type tested (Noer et al., 2022; Paulsen et al., 2018).
87 However, extra-chromosomal DNA can also be of exogenous origin. Remarkably, when
88 lambda phage or plasmid DNA was mixed with *Xenopus* oocyte extracts, it was subsequently
89 enwrapped by a nuclear envelope, which could suggest that any DNA can be enveloped by a
90 nuclear envelope (Blow & Laskey, 1986; Newport, 1987). Thus, exogenous extra-
91 chromosomal DNA introduction into cells by e.g., viral or bacterial infections or transfection
92 provide opportunities to study the formation of nucleus-like structures, as well as help to
93 understand how cells distinguish chromosomal from extra-chromosomal DNA. Therefore, in
94 this study we have introduced DNA into the cytoplasm of mammalian somatic cells and
95 characterized its enwrapping by membranes. Particularly, we investigated the similarities and
96 differences between such membranes and a bona fide nuclear envelope.

97 **Results**

98

99 **Cells sort transfected plasmid DNA to the cytoplasm**

100 We chose to study the association of plasmid DNA with membranes after its transfection into
101 human tissue culture cells, as its visualization is established. To visualize transfected plasmid
102 DNA, we used the LacO/Lacl-system, where a plasmid containing 256 repeats of the Lactose
103 (Lac) Operon (pLacO) is introduced into cells stably expressing Lac Inhibitor (Lacl) fusion
104 protein with either GFP or mCherry as fluorescence tag. Here, we employed three different
105 HeLa cell lines (hereafter referred to as “HeLa-Lacl”) and transfected them with pLacO to
106 analyze the localization of transfected plasmid DNA. Fluorescent LacI foci in the cytoplasm
107 were detected in cells transfected with plasmid DNA either by lipofection or electroporation
108 (two methods to introduce plasmid) (SFig. 1; as previously reported in (Wang et al., 2016)).
109 Due to the presence of a nuclear localization sequence (NLS) in the LacI fusion protein, the
110 nuclear LacI fluorescence generally masked signals coming from plasmids in the nucleus.
111 These results confirm that the LacI foci report plasmid localization in cells after transfection;
112 hereafter, we refer to these LacI foci as plasmid foci. We first used this reporter system to
113 study the localization and dynamics of plasmid foci. To do so we performed time-lapse live-
114 cell microscopy for up to 24 hours (Fig. 1A-D, SFig. 2, SFig. 3). We started image acquisition
115 concomitantly with the addition of the plasmid-lipofection mix to the cells and under conditions
116 that preserved viability in the dividing cell population (SFig. 2A).

117

118 We observed the formation of plasmid foci throughout the imaging period, perhaps because
119 plasmids continuously entered the cells (Fig. 1B, SFig. 2B). Most of these plasmid foci (89 %)
120 persisted throughout the entire imaging period (Fig. 1B). The other plasmid foci (11 %) were
121 visible for variable durations (between 30 min and 17 hours) before disappearing (Fig. 1B,
122 SFig. 2C). Consistent with our previous study, most cells exhibited only one plasmid focus
123 (63 %; SFig. 2D, (Wang et al., 2016)). Next, we analyzed the history of cells with a single focus
124 at the end of imaging (211 cells, 63 % of all cells with ≥ 1 plasmid foci, 19% of all imaged cells
125 at the end of imaging). Interestingly, we found that 76 % of cells with one plasmid focus had
126 either formed only a single plasmid focus or inherited it during mitosis. In contrast, partitioning
127 of multiple foci during mitosis or disappearance of foci (21 % and 3 %, respectively) contributed
128 less to the cells with one plasmid focus at the end of imaging. Notably, we did not observe any
129 plasmid foci fusion events under our imaging conditions (SFig. 2E, F; total 291 plasmid foci in
130 114 cells over up to 24 hours). These data show that transfected cells usually form only one
131 plasmid focus. Once formed, plasmid foci are generally stable.

132

133 Our live-cell imaging also revealed that 58 % of plasmid foci formed during interphase, while
134 the other 42 % were plasmid foci formed during mitosis, away from the chromosomal mass
135 (Fig. 1A, mitotic formation, bold time point, C, SFig. 2I). Amongst the plasmid foci formed
136 during interphase 88 % formed in the cytoplasm and 12 % in the nucleus (Fig. 1A, C, SFig.
137 2G). Next, we analyzed the location of each appearing plasmid focus at the end of imaging.
138 Irrespective of where and when plasmid foci formed, all but one ended up in the cytoplasm
139 (Fig. 1A at 24 h, D, SFig. 2H, I).

140

141 Next, we wondered how plasmid foci formed in the nucleus entered the cytoplasm. Focusing
142 on plasmid foci formed in the inner nucleoplasm, we observed two different translocation
143 modes: 13 out of 15 such plasmid foci entered the cytoplasm during mitosis by being sorted
144 away from the chromosomal mass (SFig. 3A (1st example), B). The other two plasmid foci left
145 the nucleus during interphase by nuclear budding (SFig. 3A (2nd example), B), revealing that
146 the cell employs at least two ways to exclude plasmid DNA from the nucleus.

147

148 These data make four points. First, most of the plasmid DNA becomes LacI-associated in the
149 cytoplasm and remains there, possibly without ever reaching the nucleus. Second, there are
150 two modes for nuclear plasmid to partition away from the chromosomes: through expulsion
151 via nuclear budding from the interphase nucleus (SFig. 3A (2nd example)) or through
152 separation from the chromosomal mass during mitosis (mitotic sorting, Fig. 1A upper panel
153 9.5 hours, and bottom panel 4.5 hours, SFig. 2I, SFig. 3A (1st example), B). Third, the sorting
154 of plasmid DNA from chromosomal DNA occurs rapidly; plasmid foci formed either during
155 mitosis or in the nucleus during interphase relocated to the cytoplasm within 1 hour after their
156 appearance (median, SFig. 3C). Fourth, in contrast to micronuclei formed by lagging
157 chromosomes or parts of them, plasmid foci formed during mitosis are predominantly formed
158 before (88 % of mitotically appearing plasmid foci) and not during anaphase, when
159 chromosomal fragments or lagging chromosomes become visible as distinct units (SFig. 3D,
160 E). Furthermore, plasmid foci unlike micronuclei never formed in the region between the
161 separating chromosomes during anaphase (Fig. 1A, mitotic formation 4.5 hours, SFig. 3D, E,
162 (Liu et al., 2018; Orr et al., 2021; Wang et al., 2016)). Therefore, we conclude that the
163 dynamics of LacI decorated plasmid DNA are distinct from the mitotic separation of
164 chromosomal fragments or lagging chromosomes from the chromosomal mass. Finally, most
165 plasmid foci are formed during interphase (58 %) and are thus not mitotic products in contrast
166 to micronuclei. Overall, these data reveal that HeLa cells have three ways to specifically sort
167 plasmid DNA away from the chromosomes and that the cell collects plasmid DNA in the
168 cytoplasm where it persists.

169

170 **Cytoplasmic plasmid foci remain separated from chromosomes over extended periods
171 of time**

172 Next, we extended the period of live cell imaging up to 122.5 hours to assess if the separation
173 between chromosomes and plasmid DNA is maintained for long time periods (Fig. 1E, F).
174 About 2/3 of the cytoplasmic plasmid foci were maintained and stayed separated from
175 chromosomes during this period, frequently being propagated over 3 cell divisions. The
176 fluorescence of about 1/3 of the foci however decayed over more than 10 hours, before
177 disappearing (Fig. 1F). Since the fluorescence decay occurred only at some plasmid foci within
178 a whole field of view, it was not due to bleaching, but suggests that the DNA was degraded
179 (SFig. 4). Cytoplasmic plasmid foci remained in the cytoplasm during the imaging period and
180 we never observed entry into the nucleus (Fig. 1E, SFig. 4), in contrast to what is reported for
181 DNA of micronuclei (Crasta et al., 2012; Zhang et al., 2015). Thus, even up to 122.5 hours
182 after transfection, plasmid foci behaved similarly to early periods after lipofection. Thus, the
183 separation between chromosomal DNA and plasmid DNA is persistent over several divisions,
184 consistent with (Wang et al., 2016).

185

186 **Cells harboring a single cytoplasmic plasmid focus are dominant under diverse
187 conditions**

188 We next studied whether these observations were time- and plasmid type-dependent and
189 occurred in other cell types. We have previously shown that most pLacO lipofected MDCK
190 cells (non-transformed canine kidney cells) predominantly had one cytoplasmic focus per cell,
191 24 hours after transfection. Here we assessed how MDCK-Lacl and HeLa-Lacl cells handled
192 plasmid DNA at different times after electroporation and lipofection (SFig. 5A-C). Two critical
193 results are highlighted here. First, in both cell lines and employing both transfection methods,
194 most cells with plasmid foci (grouped into classes of 1- and various multi-foci cells) had a
195 single plasmid focus, regardless of the time point after transfection (3 hours – 72 hours; SFig.
196 2D, SFig. 5C). Further, the analysis of the electroporation experiments shows that at 3 hours
197 the sum of all different classes of cells with multiple foci pooled together (61 %) is larger than
198 the fraction of cells with only one focus (39 %). This ratio changed over time. Notably, between
199 24 hours and 72 hours after transfection, the fraction of multi-foci cells decreased strongly,
200 while that of the 1-focus cells increased (1-focus cells: 50 % at 24 hours; 82 % at 72 hours).
201 As this occurred in the absence of further plasmid uptake - in contrast to lipofection - the data
202 suggests that either multi-foci cells died, or a single cytoplasmic focus is differentiated from
203 other plasmid foci in a cell and selectively maintained.

204

205

206 We next tested if the LacO repeat sequence had any effect on the cytoplasmic localization of
207 transfected plasmids. For this, we lipofected plasmids with and without LacO repeats and with
208 or without coding sequences into HeLa cells. Subsequently, we used FISH to visualize these
209 plasmids (SFig. 5D-F). For all tested plasmids, most focus-containing cells had a single
210 cytoplasmic focus 24 hours after lipofection, similar to our experiments where we visualized
211 pLacO with LacI fluorescence (SFig. 5E, F). These results show that plasmid DNA is
212 preferentially maintained in a single plasmid focus in the cytoplasm of mammalian cells,
213 regardless of the cell line, plasmid type, or transfection method.

214

215 **Plasmid DNA localizes to the cytoplasm in an ER-enwrapped compartment**

216 The cytoplasmic plasmid foci are ideal to assess if and which membrane is associated with
217 them. As the nuclear envelope originates from the endoplasmic reticulum (ER) and ER is
218 abundant in the cytoplasm, we first quantitatively characterized the association of plasmid
219 DNA with ER. 24 hours after pLacO lipofection into HeLa-LacI cells expressing either the ER
220 transmembrane reporter Sec61-mCherry (Fig. 2A) or the ER-lumen reporter eGFP-KDEL (Fig.
221 2B), all cytoplasmic plasmid foci colocalized with both ER reporters. Immunofluorescent
222 detection of the ER-residing LEM-domain protein LEM4 (ANKLE2) confirmed the presence of
223 ER at all cytoplasmic plasmid foci 24 hours after lipofection (Fig. 2C) or electroporation (SFig.
224 6A). The intensities of the ER-reporters KDEL and LEM4 were similar at the plasmid focus
225 compared to the overall ER in 71 % to 91 % of the cases, (category referred to as "non-
226 enriched", Fig. 2B, C, SFig. 6A). However, the intensity of the ER transmembrane marker
227 Sec61 was frequently higher at the plasmid focus compared to the overall ER (category
228 referred to as "enriched" in 61 % of the cases, Fig. 2A, SFig. 6A). Thus, ER membrane and
229 luminal ER proteins were always present at the cytoplasmic plasmid focus, suggesting that a
230 double membrane encloses the plasmid DNA, reminiscent of the nuclear envelope.

231

232 **A special double membrane enwraps cytoplasmic plasmid DNA**

233 To visualize the cytoplasmic plasmid focus at higher resolution, we used correlative light and
234 electron microscopy (CLEM) in interphase HeLa cells 24 hours after pLacO lipofection. In
235 these images, a double membrane enclosing the cytoplasmic plasmid focus is clearly visible
236 (Fig. 3A, yellow arrowheads in the blue inset) similarly to the nuclear envelope (yellow
237 arrowheads in the green inset). The membrane surrounding the plasmid focus has
238 fenestrations, indicating that it may be an open compartment (green arrowheads in the blue
239 inset). Moreover, this membrane connects to the ER (red arrowhead in the blue inset),
240 consistent with the presence of ER proteins at plasmid foci. The cytoplasmic plasmid focus
241 has a higher electron density than the interphase chromosomes in the nucleus suggesting a
242 denser DNA packing in the plasmid focus. Overall, aside from the fenestrations, this

243 compartment's membrane organization is highly reminiscent of the nuclear envelope
244 surrounding chromosomal DNA.

245

246 To further investigate the similarities between the membrane enclosing the plasmid focus and
247 the nuclear envelope, we probed for the presence of inner nuclear membrane proteins at
248 cytoplasmic plasmid foci 24 hours after transfection with pLacO. We paid particular attention
249 to those that could participate in a DNA-membrane tethering at cytoplasmic plasmid foci. One
250 tether at the nuclear envelope is composed of BAF and INM-membrane proteins with a LEM-
251 domain, like Emerin or Lap2 β (Ibrahim et al., 2011; Lee et al., 2001; Zheng et al., 2000).
252 Remarkably, cytoplasmic plasmid foci always contained BAF alongside Emerin and Lap2 β
253 (Fig. 3B, C, E) (Ibrahim et al., 2011; Kobayashi et al., 2015). BAF was in addition always
254 enriched at plasmid foci compared to the nuclear envelope suggesting a high density of
255 plasmid molecules. More remarkable is that Emerin was enriched at nearly all foci (90 %, Fig.
256 3E, SFig. 6B). Lap2 β was less frequently enriched (40 %; Fig. 3E, SFig. 6B). These results
257 suggest that LEM-domain proteins and BAF might tether plasmid DNA to surrounding ER
258 membranes. Another known tether at the nuclear envelope involves the transmembrane
259 protein Lamin B Receptor (LBR), which binds to heterochromatin protein 1, repressing
260 transcription in the nearby chromatin (Ye and Worman, 1996). LBR was not detected at
261 plasmid foci (Fig. 3D, E). Therefore, we conclude that this second DNA-membrane tether is
262 missing. Overall, the double membrane around the cytoplasmic plasmid focus has both
263 similarities (presence of Emerin and Lap2 β) and differences (fenestrations, absence of LBR,
264 enrichment of Emerin) to the nuclear envelope.

265

266 **The special double membrane enwrapping cytoplasmic plasmids is devoid of**
267 **functional NPCs**

268 Next, we probed for NPCs in the membrane around cytoplasmic plasmid foci in HeLa cells,
269 24 hours after transfection with pLacO. NPCs appear to be absent, as both FG-repeat
270 containing nuclear pore proteins (NUPs; anti-FG repeat) and Embryonic Large Molecule
271 Derived From Yolk Sac (ELYS), which is required for NPC assembly (Rasala et al., 2006),
272 were both absent from cytoplasmic plasmid foci in 94 % of the cases (Fig. 4A). The rare cases
273 when these proteins are present at the plasmid focus might reflect remnants of nuclear
274 budding events. The transmembrane protein Nuclear Envelope Pore Membrane 121
275 (POM121) was always absent at plasmid foci (Fig. 4B). We also probed for evidence of NPC-
276 mediated nuclear-cytoplasmic transport at cytoplasmic plasmid foci. Here, we observed that
277 the Importin β -binding Domain (IBB-GFP) was always absent (Fig. 4C). In addition, the
278 nucleotide exchange factor for Ran (Regulator of Chromatin Condensation 1, RCC1), which
279 supports NPC formation and establishes a Ran-gradient across the enclosing membrane, was

280 never detected at cytoplasmic plasmid foci (Fig. 4D, (Walther et al., 2003)). We conclude that
281 the double membrane enclosing cytoplasmic plasmid DNA is devoid of functional NPCs.

282

283 The EM analysis indicated that the cytoplasmic plasmid compartment is not entirely closed
284 (Fig. 3A). Therefore, we tested whether soluble GFP could access the cytoplasmic plasmid
285 compartment by Fluorescence Recovery After Photobleaching (FRAP) in HeLa-Lacl cells 24
286 hours after lipofection of pLacO. The GFP fluorescence was bleached at the cytoplasmic
287 plasmid focus and a reference area in the cytoplasm (Fig. 4 E-G). Fluorescence recovery took
288 place in both areas, with the recovery time (the time when half of the bleached signal is
289 recovered, $t_{1/2}$) being slightly longer for areas containing the plasmid focus (1.8 times),
290 showing that the diffusion of GFP molecules into the plasmid focus is hindered, but not
291 abolished. Thus, the special double membrane enclosing cytoplasmic plasmid DNA, while
292 devoid of functional NPCs, still allows exchange with the cytoplasm.

293

294 **A plasmid focus formed in the cytoplasm is rapidly enwrapped by membrane**

295 The nuclear membrane rapidly encloses chromosomal DNA at the end of mitosis. Therefore,
296 we assayed the time scale of membrane association with cytoplasmic plasmid DNA. We used
297 HeLa cells stably expressing Lap2 β -GFP and transiently expressing Lacl-mCherry without
298 NLS to ensure enough Lacl was present in the cytoplasm, allowing early cytoplasmic plasmid
299 visualization. In addition, the cells were thymidine-synchronized to ensure a higher
300 homogeneity of the cell population. These cells were lipofected with pLacO and imaged every
301 15 min for 25.25 hours starting after the addition of the lipofection-DNA mix to analyze
302 appearing plasmid foci (Fig. 5). 51 % of such plasmid foci were already associated with
303 membrane at their appearance, as reported by Lap2 β (Fig. 5D). Over time, plasmid foci were
304 increasingly associated with Lap2 β -containing membrane. Finally, 75 min after appearance,
305 97 % of the plasmid foci were Lap2 β -membrane-associated (Fig. 5D). Thus, membrane
306 association appears to accompany plasmid focus appearance (Fig. 5C, D).

307

308 **Emerin is enriched at cytoplasmic plasmid compartments in primary human cells**

309 To probe if the special double membrane can also form around cytoplasmic plasmid foci in
310 non-immortalized cells, we transfected primary human fibroblasts with pLacO and visualized
311 the plasmid with transiently expressed Lacl-NLS-GFP. In addition, we immunostained the cells
312 for Emerin or LEM4 (Fig. 6A, B). We noticed that these primary cells divided significantly less
313 frequently than HeLa cells and therefore analyzed the cells 48 hours after pLacO transfection.
314 Also here, most transfected cells had a single plasmid focus (SFig. 6C). Emerin was present
315 at each plasmid focus amongst cells with one plasmid focus and even enriched in 97 % of the
316 instances compared to the surrounding ER or nuclear envelope (Fig. 6A). Also, all plasmid

317 foci in multi-foci cells were Emerin positive apart from one cell, where three foci didn't
318 colocalize with Emerin, possibly because the reaction to transfection is delayed in these
319 primary cells compared to HeLa cells (SFig. 6D). Remarkably, in multi-foci cells, several
320 plasmid foci of a single cell were Emerin enriched (SFig. 6D, F). Similarly, LEM4 was always
321 present in cells with one plasmid focus and, in 45 % of these cells, even enriched compared
322 to the surrounding ER. This is qualitatively similar to HeLa cells (Fig. 6B). In multi-foci cells
323 LEM4 was always present, except for 2 plasmid foci in two different cells (SFig. 6E).

324

325 Thus, both in primary human fibroblasts as well as in HeLa cells, plasmid DNA is excluded
326 from the nucleus and localizes to the cytoplasm where it exists predominantly in one
327 membranous organelle. We term this organelle the exclusome. A diagnostic hallmark of the
328 exclusome is that Emerin is enriched as compared to the nuclear envelope. The exclusome
329 envelope is further characterized by the presence of fenestrations, presence of Lap2 β ,
330 presence and even occasional concentration of ER-membrane proteins like Sec61 or LEM4,
331 and the absence of NPCs and LBR.

332

333 **Interference with Emerin's function reduces the compartmentalization of plasmid DNA 334 in the cytoplasm**

335 Since Emerin is enriched at ~90 % of plasmid foci and the formation of a double membrane is
336 concomitant with plasmid focus formation (Fig. 3B, E, Fig. 5), we speculated that Emerin might
337 tether plasmid DNA to the surrounding membrane to establish an exclusome. As Emerin's
338 LEM-domain binds BAF and BAF binds DNA (Lee et al., 2001), we aimed to interfere with this
339 molecular linkage. To do so, we chose to interfere with the function of Emerin's LEM-domain
340 by setting up a competition approach with an excess of the soluble LEM-domain of Emerin.
341 Specifically, we overexpressed either the LEM-domain of Emerin fused to GFP and a nuclear
342 export signal ("GFP-LEM") or soluble GFP ("GFP") (Fig. 7A, left side) as a control in
343 synchronized HeLa-LacI cells. Subsequently, pLacO was electroporated and cells that
344 expressed GFP-LEM or GFP were analyzed (Fig. 7A, right side). The competition was
345 successful for two reasons. First, Emerin was less enriched at the nuclear envelope and more
346 present in the ER in cells expressing GFP-LEM compared to control cells expressing GFP.
347 This suggests that the overexpression of GFP-LEM competed with endogenous Emerin for
348 DNA tethering at the nuclear envelope, thus leading to reduced Emerin retention at the nuclear
349 envelope and re-localization to the ER (SFig. 7B, C). Second, Emerin associated also less
350 frequently with cytoplasmic plasmid foci at two time points after pLacO transfection in cells
351 expressing GFP-LEM compared to the control (Fig. 7B, SFig. 7D).

352 The amino acid sequences of the LEM-domains of Emerin and LEM4 are 44 % similar (SFig.
353 7A). Because of this, the overexpressed LEM-domain of Emerin might also interfere with the

354 function of other LEM-domain proteins. To test for this possibility and to further characterize
355 the plasmid focus membrane, we probed for the presence of LEM4. The association of LEM4
356 was not affected in GFP-LEM expressing cells at either 6 hours or 24 hours after pLacO
357 electroporation (Fig. 7C, SFig. 7E). Moreover, LEM4 was present in all conditions at almost
358 all cytoplasmic plasmid foci (99 %, mean of 3 to 5 exp., all conditions), revealing that even
359 Emerin-negative plasmid foci are membrane-enclosed. Furthermore, the presence of LEM4
360 in Emerin-negative plasmid foci indicates that other proteins might compensate for Emerin's
361 function, although clearly less efficiently.

362

363 Since we could interfere with Emerin's function, we went on to characterize the effects of GFP-
364 LEM overexpression on the cell's reaction towards transfected plasmid DNA. We determined
365 how many cells expressing GFP-LEM or GFP, had at least one cytoplasmic plasmid focus. In
366 the GFP-LEM condition, fewer cells contained at least one cytoplasmic plasmid focus. In
367 compared to control, both 6 hours and 24 hours after pLacO transfection (36 % for GFP-LEM
368 and 66 % for GFP; Fig. 7D). At 24 hours after transfection, the number of cells with plasmid
369 foci were halved in both conditions compared to the 6-hour time point due to cell division and
370 asymmetric partitioning of the plasmid foci (16 % for GFP-LEM and 35 % for GFP). Together,
371 these data suggest that Emerin, through its LEM-domain, supports the compartmentalization
372 of plasmid DNA within the cytoplasm of mammalian cells.

373

374 **Exclusomes can contain telomeric DNA**

375 In cells undergoing alternative lengthening of telomeres (ALT), like the osteosarcoma cell line
376 U2OS, circular extra-chromosomal DNA of telomeric origin is abundant (Cesare and Griffith,
377 2004). Remarkably, in U2OS and several other cancer cell lines, such as WI38-VA13, SaOs2,
378 and KMST-6, between 1 and 4 FISH signals of extra-chromosomal telomeric DNA were
379 detected in the cytoplasm (Chen et al., 2017; Tokutake et al., 1998). In addition, several
380 groups have detected circular extra-chromosomal telomeric DNA in non-ALT cancer cells like
381 HeLa (Regev et al., 1999; Tokutake et al., 1998; Vidaček et al., 2010; Wang et al., 2004).
382 Therefore, we decided to test whether this extra-chromosomal DNA of endogenous origin is
383 membrane-enclosed in the cytoplasm and whether this membrane shares similarities with the
384 nuclear envelope or the exclusome.

385

386 We performed FISH experiments in U2OS and HeLa cells using two different fluorescently
387 tagged telomeric probes (TelC and TelG). In all cases, we observed numerous FISH signals
388 in the nuclei and few in the cytoplasm (Fig. 8A, B, SFig. 8A, B). We also demonstrated that
389 the cytoplasmic Tel FISH signals were not artifacts caused by clustered probes as cells
390 simultaneously hybridized with both a telomeric probe as well as a scrambled probe only

391 showed telomeric probes signals (SFig. 8A-C). Further, both types of cytoplasmic telomeric
392 FISH signals indeed labeled DNA, as a DNaseI treatment prior to probe hybridization
393 abolished the signal (SFig. 8D, E).

394

395 Micronuclei with chromosomal fragments frequently occur in cancer cells. To exclude such
396 compartments from our analysis, we chose Hoechst fluorescence as a criterium, as the
397 median size of circular ex-tDNA is only 5 kb (Cesare and Griffith, 2004). Based on this criterium,
398 we distinguished two types of tDNA in the cytoplasm of both HeLa and U2OS cells: tDNA in
399 Hoechst positive foci, termed micronuclear tDNA (MN tDNA, Fig. 8A (grey squares)) as they
400 might contain chromosomal DNA fragments with telomeres; and extrachromosomal tDNA
401 without Hoechst stain, termed ex-tDNA. In the following analyses, we focused on the
402 cytoplasmic ex-tDNA (Fig. 8A (yellow squares)). Overall, there were fewer cells with ex-tDNA
403 foci in the HeLa population (7 - 16 %) compared to the U2OS population (36 - 48 %, SFig. 8C).
404 Such a difference is expected for non-ALT cells versus ALT-cells and is consistent with the
405 notion that ex-tDNA foci represent circular ex-tDNAs. Remarkably, both HeLa and U2OS cells
406 mostly contained one ex-tDNA focus per cell for both types of probes (U2OS 25 %, HeLa 5 %),
407 which is strikingly similar to our findings with transfected plasmid DNA ((Wang et al., 2016),
408 Fig. 8B).

409

410 Next, we analyzed whether cytoplasmic ex-tDNA foci are membrane-enclosed in U2OS cells.
411 We could not directly probe for the presence of Emerin, as none of our anti-Emerin antibodies
412 sustained the conditions used in FISH-IF experiments. However, overexpressed Sec61-
413 mCherry colocalized with 47 % of ex-tDNA foci but always colocalized with MN tDNA (Fig. 8C,
414 SFig. 8F). Also, Lap2 β was present at 41 % of ex-tDNA foci but always present at MN tDNA
415 foci (Fig. 8D, SFig. 8F). ELYS was never present at ex-tDNA foci but was typically present at
416 MN tDNA (2 out of 3 cases) (Fig. 8E, SFig. 8F). Thus, the co-localization frequencies for the
417 tested ER- and INM-proteins at ex-tDNAs were lower as for plasmid foci, possibly due to the
418 reduced focus size (Fig. 8A, C-E, yellow squares) and the harsh conditions applied during
419 FISH. Notably, NPCs were absent from ex-tDNA but not from tDNA in micronuclei (Fig. 8E,
420 SFig. 8F), consistent with the possibility that the latter are formed during mitosis and have
421 different contents than ex-tDNA foci. Collectively, these results indicate that ex-tDNA can also
422 be contained in exclusomes.

423

424

425 **Both plasmid DNA and ex-tDNA cluster in an exclusome**

426 Due to the observed similarities between ex-tDNA and plasmid DNA, we tested if they
427 colocalize within the same exclusomes. U2OS cells were fixed and immunostained for Lap2 β

428 24 hours after lipofection with pLacO. In addition, the cells were hybridized *in situ* with probes
429 for both LacO and TelC. Indeed, plasmid and ex-tDNA colocalized in the cytoplasm in one
430 Lap2 β containing membrane compartment (Fig. 9A). Among all cells with both types of DNA
431 in the cytoplasm (co-existence cells), 26 % had both DNA types in a single cytoplasmic
432 compartment (Fig. 9B, single exp. SFig. 8G). 75 % of such compartments contained Lap2 β in
433 their envelope (Fig. 9A, C, SFig. 8H). In 74 % of such Lap2 β -containing compartments plasmid
434 and tDNA foci were Hoechst positive, which could represent chromosomal fragments with
435 telomeres together with plasmid DNA (Fig. 9C, SFig. 8H). However, the fact that 26 % of such
436 compartments were Hoechst negative reveals that ex-tDNA, and not telomeric DNA from
437 chromosomal ends, colocalized with plasmid DNA in one cytoplasmic membrane-bound
438 compartment (Fig. 9A). Therefore, we conclude that extra-chromosomal DNAs of different
439 origins, such as endogenous telomeric DNA and exogenous plasmid DNA, can cluster in one
440 exclusome (Fig. 9D).

441 **Discussion**

442

443 Our study reveals that somatic vertebrate cells maintain transfected DNA in a new structure,
444 which we term exclusome and which represents a third cytoplasmic DNA compartment
445 besides the nucleus and mitochondria. The exclusome, mostly one per cell, is a cytoplasmic
446 membranous compartment into which the cell sorts and where it retains transfected plasmid
447 and extra-chromosomal elements, such as telomeric DNA, likely in circular form, for extended
448 periods of time. 24 hours after transfection, the envelope of the exclusome strikingly resembles
449 the nuclear envelope in some aspects but differs from it in others (Fig. 9D). Thus, a nuclear-
450 like envelope was assembled around cytoplasmic plasmid DNA. We observed this in the
451 variety of cells studied here (HeLa, U2OS, MDCK, primary human fibroblasts), suggesting it
452 is not cell type specific amongst somatic cells. This is remarkable, as it enlarges our
453 understanding of the formation of the nucleus and the nuclear envelope.

454

455 The exclusome and the nucleus have three striking similarities. Both contain DNA and exist
456 generally each as a single unit in the cell. In both cases their membranous envelope is a sheet-
457 like double membrane derived from the ER (as shown by the presence of Sec61, LEM4, and
458 KDEL-GFP) and comprising specific INM proteins (Lap2 β and Emerin). These points suggest
459 that bringing DNA together in one unit and enwrapping it with a minimal ER-derived double
460 membrane containing Lap2 β and Emerin might represent a default response to DNA
461 (Kobayashi et al., 2015).

462

463 However, there are also clear differences distinguishing the exclusome from the nucleus: its
464 envelope structure and its DNA content. The envelope of the exclusome differs from that of
465 the nucleus, as LBR and NPCs are missing, Emerin is enriched, and membrane fenestrations
466 are present in the exclusome envelope but not in the nuclear envelope. At the end of mitosis,
467 Lap2 β and Emerin, are known to arrive within the first membrane patches that assemble on
468 the decondensing chromosomes (Haraguchi et al., 2008). In contrast, complete NPCs are only
469 very late in telophase in the membrane wrapping around the chromosomes (Haraguchi et al.,
470 2000; Otsuka et al., 2018; Otsuka et al., 2023). Similarly, the sealing of fenestrations does not
471 occur in the envelope of the exclusome however it does occur during the formation of the
472 nuclear envelope late in mitosis (Ventimiglia et al., 2018). Thus earlier, but not later steps of
473 nuclear envelope formation concur to generate the exclusome. Remarkably plasmid DNA
474 competed in *in vitro* assays with nuclear envelope formation around chromosomes (Ulbert et
475 al., 2006). Therefore, it could become a useful model for identifying the triggers establishing
476 the contacts between protein containing membrane and DNA, the first steps of nuclear
477 envelope assembly.

478

479 Another difference is the enrichment of Emerin in the envelope of the exosome compared to
480 the nuclear envelope (Haraguchi et al., 2022; Ibrahim et al., 2011; Kobayashi et al., 2015).
481 This hallmark characteristic is in striking contrast to micronuclei, which contain chromosomal
482 fragments or entire chromosomes, as their surrounding membrane is enriched for Lap2 β but
483 not for Emerin (Liu et al., 2018). Emerin's enrichment might be due to liberation of Emerin from
484 the INM as seen upon stress (Buchwalter et al., 2019), or is due to accumulation of ER
485 membrane with newly synthesized Emerin at the site of exosome formation, similarly as seen
486 for the envelopment of chromosomal fragments (Ferrandiz et al., 2022). Our results further
487 suggest that Emerin and its LEM-domain play a key role in the envelopment of plasmid DNA
488 in the cytoplasm. What drives Emerin specificity for exosomes, in contrast to LEM4 for
489 example, remains to be investigated. Intriguingly the DNA-viruses, vaccinia virus and
490 mimivirus, generate replication factories from the ER in the host cell cytoplasm (Greseth and
491 Traktman, 2022; Mutsafi et al., 2013). It will be interesting to determine whether the ER at
492 these factories shows similarities to that at the exosome.

493

494 What do these differences possibly mean? Besides NPCs, we noticed that RCC1 and ELYS
495 were both absent from exosomes. Both regulate early steps of NPC formation (Gómez-
496 Saldivar et al., 2016; Walther et al., 2003) and their absence might explain why exosomes
497 do not assemble NPCs. The absence of ELYS would explain that of LBR from exosomes as
498 well (Mimura et al., 2016). Thus, it will be interesting to determine what causes the absence
499 of ELYS and RCC1 from exosomes. Possibly, it is due to differences in chromatinization of
500 the DNA in the exosome compared to that of chromosomes in the nucleus, to which RCC1
501 binds (Chen et al., 2007). Remarkably, human artificial chromosomes (HAC) relocalize to a
502 cytoplasmic "nanonucleus" upon inactivation of their engineered centromere (Nakano et al.,
503 2008). These nanonuclei have not been further characterized. Yet, it is tempting to speculate
504 that the absence of a centromere on a DNA molecule might be signal to sort that DNA into an
505 exosome. Future studies will determine the molecular determinants governing how a given
506 DNA molecule is enveloped and thus how the cell distinguishes extra-chromosomal DNA like
507 plasmid and ex-tDNA from the chromosomes.

508

509 The content of the exosome differs from that of the nucleus. We reveal processes, by which
510 the cell actively separates chromosomal from extra-chromosomal DNA. The cell sorts
511 transfected plasmid DNA and ex-tDNA into the exosome, whereas it bundles the
512 chromosomes into the nucleus at the end of mitosis. We show that sorting of incoming plasmid
513 DNA likely occurs directly in the cytoplasm, as most plasmid foci are formed in this
514 compartment. Thereby, only little plasmid DNA reached the nucleus under our transfection

515 and visualization conditions. In this regard, the exclusome prevented contact between the
516 transfected DNA and the chromosomal DNA. When the transfected DNA reached the nucleus,
517 it did not remain there, but was expelled. We identified two modalities by which nuclear
518 plasmids became separated from chromosomal DNA, which remove plasmid from the nucleus,
519 where it is generally thought to be expressed. The first one, mitotic sorting, expels plasmid
520 DNA to the cytoplasm during mitosis. This mechanism was also reported for plasmid DNA
521 microinjected into the nucleus (Ludtke et al., 2002). The second one occurs during interphase
522 and involves the budding of a newly formed exclusome out of the nuclear envelope, into the
523 cytoplasm. Similar, chromosome-derived large circular DNAs encoding c-myc visualized by
524 FISH localized in nuclear buds in the human colorectal adenocarcinoma cancer cell line COLO
525 320DM (Shimizu et al., 1998). In all cases, the transfected DNA and even originally nuclear
526 ex-tDNA end up in a cytoplasmic exclusome. Thus, the cell has a machinery distinguishing
527 and sorting these DNAs from chromosomal DNA.

528

529 Cells maintain an exclusome with plasmid DNA for long periods of time over multiple cell
530 divisions, but the physiological relevance of this is unknown. Generally, cytoplasmic DNA is
531 sensed as a danger signal by the cyclic guanosine monophosphate–adenosine
532 monophosphate synthase (cGAS), which provokes type I interferon production to warn
533 neighboring cells about this rogue DNA. The organismal immune system would subsequently
534 remove such a cell. As cGAS was found at transfected cytoplasmic plasmid DNA, the
535 exclusome might be an immunologically relevant signaling hub until the cell is eliminated
536 (Guey et al., 2020). Additionally, an exclusome might alter the cellular reaction to other
537 incoming DNAs and could explain why transfection or virus infection are less efficient
538 subsequently to a first transfection (Grandjean et al., 2011; Langereis et al., 2015). In such a
539 scenario, we suggest that the exclusome might act as a memory deposit for both systemic
540 and cell-autonomous immunity towards DNA. In line with this, DNA enwrapping seems to be
541 in competition with nucleases, as most of the transfected DNA is likely degraded before being
542 captured in an exclusome (Shimizu et al., 2005). Also, plasmid foci occasionally disappeared
543 over time, indicating that the maintenance of an exclusome is constantly challenged by cellular
544 defense processes.

545

546 To conclude, we identified that cells distinguish, sort, and cluster extra-chromosomal DNAs
547 away from their chromosomes into a membranous compartment in the cytoplasm, the
548 exclusome. The envelope of the exclusome bears some similarities to the nuclear envelope
549 but also differences as it e.g., does not perform the NPC-controlled nucleo-cytoplasmic
550 exchange of the nuclear envelope. Remarkably, most exclusomes form in interphase cells,
551 whereas the nucleus of mammalian cells forms specifically at mitotic exit. This suggests that

552 DNA clustering and the steps of nuclear envelope formation that are common to the
553 exclusome and the nucleus are not dependent on cell cycle regulation. We suggest that they
554 may have evolved together with open mitosis as a mechanism to exclude extra-chromosomal
555 DNA from the nucleus. Indeed, following transfected plasmid DNA in budding yeast,
556 undergoing closed mitosis, revealed that exclusomes are not present (Denoth-Lippuner et al.,
557 2014; Shcheprova et al., 2008). Still, is the exclusome biology conserved in other, especially
558 non-vertebrate, organisms? We expect it to be especially prominent in organisms undergoing
559 open mitosis and in which cGAS or an analogous system is present.

560 **Material and methods**

561

562 **1. Mammalian cell lines**

563 All cell lines listed in the following were cultured at 37 °C with 5 % CO₂ in a humidified incubator
564 in the indicated media.

565

566 **1.1. HeLa**

567 HeLa Kyoto (HeLa K) (internal Lab ID: MMC278), human cervical cancer cells were a kind gift
568 from P. Meraldi (ETHZ, Switzerland) and originated from S. Narumiya, (Kyoto University,
569 Japan). Cells were cultured in Dulbecco's modified medium (DMEM) with high glucose (Gibco;
570 Thermo Fisher Scientific, Basel, Switzerland) plus 10 % FCS (PAA Laboratories; Pasching,
571 Austria) and P/S (100 U/ml penicillin and 100 mg/ml streptomycin; Gibco, Thermo Fisher
572 Scientific). Results with HeLa K are shown in Fig. 8A, B, SFig. 8A, C.

573 HeLa K cells stably expressing a mutant form of LacI that cannot tetramerize in the fusion
574 proteins LacI-NLS-mCherry (internal Lab ID: MMC114) and LacI-NLS-EGFP (EGFP,
575 enhanced GFP, internal Lab ID: MMC105) were described in (Wang et al., 2016). Cells were
576 cultured as HeLa K cells, but the medium contained in addition 5 µg/ml Blasticidin S (Gibco).
577 Both LacI-NLS-XFP cell lines, as well as HeLa transiently expressing LacI-mCherry are
578 referred to "HeLa-Laci" throughout the result and legend text. Results with HeLa LacI-NLS-
579 EGFP are shown in Fig. 2A, C, Fig. 3B, SFig. 1, SFig. 4, SFig. 5C, E, F. Results with HeLa
580 LacI-NLS-mCherry are shown in Fig. 2B, Fig. 3A, C, Fig. 4A-D, Fig. 7, SFig. 1, SFig. 7. HeLa
581 K cells transiently expressing LacI-mCherry were used in Fig. 4E-G, Fig. 5.

582 HeLa K cells stably expressing LacI-NLS-EGFP which were in addition MOCK electroporated,
583 is termed "Control HeLa" (internal Lab ID: MMC248) in SFig. 1 but otherwise "HeLa-Laci" to
584 facilitate readability. Cells were cultured like HeLa K cells, but the medium contained
585 additionally 5 µg/ml Blasticidin S (Gibco). Results with this cell line are shown in Fig. 1, SFig.
586 1, SFig. 2, SFig. 3.

587 HeLa K cells stably expressing aa 244–453 of Lap2β-GFP (internal Lab ID: MMC84), were
588 kindly provided by U. Kutay and originated from (Mühlhäuser and Kutay, 2007). Results with
589 this cell line are shown in Fig. 5. Expressed aa 244–453 of Lap2β-GFP is termed "Lap2β".

590

591 **1.2. MDCK**

592 MDCK II (Madin-Darby canine kidney) cells stably expressing LacI-NLS-EGFP (internal Lab
593 ID: MMC100), hereafter termed MDCK-Laci, were described in (Wang et al., 2016). Results
594 with this cell line are shown in SFig. 5A-C.

595

596

597 **1.3. U2OS**

598 U2OS osteosarcoma cells (internal Lab ID: MMC95), were a kind gift from C. Azzalin (Instituto
599 de Medicina Molecular, Portugal, cells originated from A. Londono Vallejo). Cells were cultured
600 in Dulbecco's modified medium (DMEM) with high glucose (Gibco) plus 10 % FCS (PAA
601 Laboratories), P/S (Gibco). Results with this cell line are shown in Fig. 8, Fig. 9, SFig. 8B-H.

602

603 **1.4. Primary human fibroblasts**

604 Human primary foreskin fibroblasts (internal Lab ID: MMC281) were kindly provided by Dr.
605 Hans-Dietmar Beer, University of Zurich, Switzerland. The foreskin had been collected with
606 informed written consent of the parents in the context of the Biobank project of the Department
607 of Dermatology, University of Zurich, and its use had been approved by the local and cantonal
608 Research Ethics Committees. Cells were cultured in Dulbecco's modified medium (DMEM)
609 with high glucose (Gibco) plus 10 % FCS (PAA Laboratories) and P/S (Gibco). Results with
610 these cells used at passage number 6 and 7 are shown in Fig. 6, SFig. 5C-F.

611

612 **1.5. Cell cycle synchronization**

613 HeLa cells were synchronized using a double thymidine (2 mM, Sigma Aldrich; St. Lewis,
614 Missouri) treatment. Cells were treated with thymidine for 16 hours, released for 8 hours and
615 treated with thymidine a second time for 20 hours. 1 hour after the second thymidine release,
616 pLacO transfection was performed. 6 hours after pLacO transfection cells were washed with
617 20 U/ml heparin in PBS (3 x 3 min, 37°C). This procedure was used in: Fig. 2A, B, Fig. 3B, D,
618 Fig. 4B-E, Fig. 5.

619 In a second thymidine treatment protocol, cells were treated with thymidine (2 mM, Sigma
620 Aldrich) for 16 hours, then released for 8 hours. 1 hour after this release, plasmids (GFP, GFP-
621 LEM) were lipofected. Cells were exposed to a second thymidine treatment (2 mM) for 18
622 hours. Cells were electroporated with pLacO 2 hours after the second thymidine release. This
623 procedure was used in Fig. 7 and SFig. 7.

624 **2. Plasmid**

625 **2.1. Oligonucleotides used**

internal Lab ID	Sequence 5'-3'
OLIGO273	CCCAAGCTCTGATTCTGTGGATAACCGTATTAC
OLIGO274	TCCCCCGGGTAAGATACATTGATGAGTTGG
OLIGO320	GGAATTCCCATGACAACCTCCAAAAG
OLIGO309	GGTGGATCCCTACAAGAAG
OLIGO328	CTAGCTAGCATGGTGAACGTGAAGC
OLIGO329	CGGGGATCCCAGGCTGCTTCTGGACACCT
OLIGO330	CAGCCATGCTGGTGGCCA

626

627 **2.2. Plasmid preparation**

628 Plasmid DNA was extracted from *E. coli* bacteria (XL1Blue strain or DH5 α strain) using
629 plasmid extraction kits (QIAGEN; Venlo, Netherlands or Macherey Nagel; Düren, Germany).
630 The DNA was purified using either Phenol/Chloroform/Isopropanol, ethanol, or 2-Propanol
631 purification. The purified DNA pellet was resuspended in ddH₂O of appropriate volume.
632 Plasmid concentration was measured by a NanoDrop Spectrophotometer (Thermo Fisher
633 Scientific).

634

635 **2.3. Construction of plasmids**

636 pControl 1 is also termed pSR9vector-CMV-mCherry (internal Lab ID: PLA1036): CMV-
637 mCherry-SV40-PA was amplified via PCR and the OLIGO273 and OLIGO274 from p-
638 mCherry-N1 without multiple cloning site (modified Clontech, Takara; United States. Internal
639 Lab ID: PLA1029). The PCR product for CMV-mCherry was cloned into the backbone of
640 pLacO (internal Lab ID: PLA977), after removing the LacO repeats.

641 pLacI-mCherry (no NLS) (internal Lab ID: PLA1107): LacI was amplified with PCR from LacI-
642 NLS-mEGFP (internal Lab ID: PLA978) using OLIGO328 and OLIGO329 with restriction sites
643 for NheI and BamHI. The backbone vector pIRESpuro2-FLAG-mCherry (internal Lab ID:
644 PLA768, kindly gifted from Yves Barral (IBC, ETH Zurich, Switzerland)) was digested with
645 NheI and BamHI and LacI PCR insert was ligated. Clones were checked with sequencing
646 using OLIGO330.

647 pEGFP-LEM-nes (internal Lab ID: PLA1098): The sequence of human Emerin's LEM-domain
648 with a nuclear exclusion signal (nes)(GGAATTCTCCGAAGATATGGACAACACTACGCAGATCTTCG
649 GATACCGAGCTGACCACCTTGCTGCGCCGGTACAACATCCGCACGGGCCTGTAGTAGGATCAACTCG
650 TAGGCTTACGAGAAGAAGATCTCGAGTACGAGACCCAGAGGCGGCGGGCCGGATTAGCCTGA
651 AATTAGCAGGTCTTGATATCTACCCGAAGATTAAGCGGCCGCTAACTAT) (internal Lab ID: SYN2)
652 was ordered from Lifetechnologies AG (Basel, Switzerland) and inserted into a modified
653 version of pEGFP-N1 (internal lab ID: PLA328).

654 pEGFP-BAF (internal Lab ID: PLA1089): BAF was amplified by PCR from pEGFP-HIS-BAF
655 (internal Lab ID: PLA1080; was a kind gift from Tokuko Haraguchi (National Institute of
656 Information and Communications Technology 588-2 Iwaoka, Iwaoka-choNishi-ku, Kobe 651-
657 2492, Japan)) with the primers OLIGO320 and OLIGO309, digested with EcoRI + BamHI, and
658 inserted into pEGFP-HIS-BAF (internal Lab ID: PLA1080).

659

660 **2.4. Plasmids used**

Plasmid	Source	internal Lab ID	Used in
pEGFP-BAF	this study	PLA1089	Fig. 3C,E
pEGFP-C1	Clontech, Takara	PLA240, PLA997	Fig. 4E-G, Fig. 7, SFig. 7B-E
pEGFP-HIS-BAF	T. Haraguchi (Shimi et al., 2004)	PLA1080	Cloning of PLA1089
p-EGFP-IBB	D. Gerlich (Schmitz et al., 2010)	PLA1061	Fig. 4C
p-EGFP-KDEL	A. Helenius (IBC, ETH Zurich, Switzerland)	PLA936	Fig. 2B
pEGFP-LEM-NES	this study	PLA1098	Fig. 7, SFig. 7B-E
pEGFP-N1	Clontech, Takara, USA	PLA328	Cloning of PLA1098
pEGFP-N3-RCC1	Y. Zheng (Li et al., 2003)	PLA1074	Fig. 4D
p-EGFP-POM121	J. Ellenberg (Beaudouin et al., 2002)	PLA1071	Fig. 4B
pIRESpuro2-FLAG-mCherry-Lacl	this study	PLA1107	Fig. 4E-G, Fig.5
pIRESpuro2-FLAG-Lacl-NLS-mCherry	Y. Barral (IBC, ETH Zurich, Switzerland)	PLA976	Fig. 6, SFig. 6C-F
pLacl-NLS-mEGFP	(Wang et al., 2016)	PLA978	Fig. 6, SFig. 6C-F
pLacO	S. M. Gasser, (Rohner et al., 2008), as in (Wang et al., 2016)	PLA977	Fig. 1-9, SFig. 1-8
p-mCherry-Sec61 β	T. Kirchhausen; (Lu et al., 2009)	PLA948	Fig. 2A, Fig. 8C
p-mCherry-N1 without multiple cloning site	modified from Clontech, Takara, USA		Cloning of PLA1036
pMLBAD (pControl2)	A. Nägele (Lefebvre and Valvano, 2002)	PLA1069	SFig. 5D-F
pSR9vector-CMV-mCherry (pControl1)	this study	PLA1036	SFig. 5D-F

661

662

663

664 **2.5. Plasmid transfection**

665 **Lipofection:** Plasmid was lipofected into cells using X-tremeGENE 9 DNA Transfection
666 Reagent (Roche; Basel, Switzerland). The plasmid:transfection reagent ratio (w:v) was 1:3.
667 Plasmid DNA concentration was either 25 ng (Fig. 2A, B, Fig. 3, Fig. 4, Fig. 5, Fig. 8, Fig. 9,
668 SFig. 8, SFig. 5C HeLa, E, F), 100 ng (Fig. 1, Fig. 2C, Fig. 6A-D, Fig. 7, SFig1, SFig. 2, SFig.
669 3, SFig. 5, SFig. 6A, SFig. 7), or 330 ng (SFIG. 5 MDCK part) per cm² cell culture dish area.
670 For double transfections (Fig. 4E-G, Fig. 6, SFig. 6C-F) plasmids were mixed in a 1: 1 ration
671 and transfected at total 100 ng/cm² cell culture dish area. To wash away excess transfection
672 mix cells were washed with 20 U/ml heparin (Sigma Aldrich, Switzerland) 6 hours after
673 lipofection in Fig. 3B-D, Fig. 4A-D, SFig. 6B. In all other condition, the lipofection mix was left
674 to incubate with the cells for the time mentioned.

675 **Electroporation:** Electroporation was conducted by a MicroPorator (AxonLab; Baden,
676 Switzerland) with Neon Transfection system 10 µL Kit (Invitrogen; Waltham, Massachusetts,
677 United States). The electroporation parameters were 1000 V, 30 ms and 2 pulses for 10 µL
678 electroporation tips using 250 ng DNA per 10⁵ suspension cells in R-buffer. Electroporated
679 cells with same condition were collected in a tube and then seeded on cover slips (SFIG. 1B,
680 SFig. 5A, B, Fig. 7, SFig. 7),

681

682 **3. FISH**

683 **3.1. FISH probes**

684 **FISH probes of PNA quality**

probe	5' end fluorescent label	Sequence 5' -3'	Company
TelG	Tamra	TTAGGGTTAGGGTTAGGG	Biosynthesis
TelC	Cy5	CCCTAACCTAACCTAA	Panagene
LacO	Alexa 488	GAATTGTGAGCGGATAACAAATT	Panagene
scramble	Alexa 488	GGGTAGGAGGTTAGTGTGTTGAGT	Panagene

685 **Other FISH probes** were generated with nick-translation method, with Alexa 568-dUTP
686 (Invitrogen), according to manufacturer's instructions on indicated template DNAs.

687

688 **3.2. DNase I enzyme treatment prior to FISH**

689 U2OS and HeLa K cells were fixed with methanol (Supelco; Bellefonte, Pennsylvania, United
690 States) for 10 min at -20 °C and then washed three times in 1x PBS. Cells were permeabilized
691 with 0.5 % Triton X-100 (Sigma-Aldrich, St. Louis, Missouri, United States) for 10 min, then
692 incubated with 0.5 unit/µL DNase (BioConcept; Allschwil, Switzerland) in 1 x PBS for 2 to 2.5
693 hours at 37 °C.

694

695

696 **3.3. Regular FISH**

697 Method modified from (Lansdorp et al., 1996). Cells were rinsed briefly in PBS before fixation.
698 The cells were fixed in 2 % paraformaldehyde (Polyscience; Hirschberg an der Bergstrasse,
699 Germany) in 1x PBS pH 7.4 for 10 min at room temperature (RT) or in 100 % methanol for 10
700 min at -20 °C. Cells were rinsed in 1x PBS three times for 5 min and fixed again for 10 min in
701 methanol at -20 °C if they were fixed with 2 % PFA before. Cells were permeabilized with 0.2
702 % Triton X-100 for 10 or 20 min, then treated with PBS containing 20 mg/ml RNase (Thermo
703 Fisher Scientific) at 37 °C for 30 min to 1 h. PNA probes were diluted to 20 nM concentration
704 in hybridization solution (70 % deionized formamide (Eurobio; Paris, France), 0.5 % blocking
705 reagent (Roche), 10 mM Tris-HCl (pH 7.2)). The DNA was denatured at 80 °C for 3 or 15 min.
706 And then incubated in a humid chamber in the dark for 2 hours at RT. Cells were washed with
707 hybridization wash solution 1 (10 mM Tris-HCl (pH 7.2), 70 % formamide and 0.1 % BSA
708 (Gerbu; Gaiberg, Germany)) for two times, 15 min each time at RT and with hybridization wash
709 solution 2 (100 mM Tris-HCl (pH 7.2), 0.15 M NaCl and 0.08 % Tween-20 (Sigma-Aldrich))
710 for three times. The nuclei were stained by Hoechst33342 (Thermo Fisher Scientific) for 3 min
711 at RT in 1 x PBS and rinsed once with 1x PBS. Cover slips containing cells were mounted in
712 Mowiol 4-88 (Sigma Aldrich) containing 1.4 % w/v DABCO (Sigma Aldrich), sealed with nail
713 polish. This method was applied for the results shown in Fig. 8A, B, SFig. 5E, F, SFig. 8 A-E.

714 **3.4. IF-FISH**

715 After the RNase treatment, cells were blocked with 5 % BSA in 1 x PBST for 1 hour at RT.
716 Then cells were incubated in primary antibody diluted in 1% BSA in 1 x PBST in a humidified
717 chamber for 1 hour at RT. Incubation with the secondary antibody (1:500 for each) in 1 % BSA
718 / 1 x PBST for 1 hour at RT in the dark. Cells were fixed with 4 % paraformaldehyde for 7 min,
719 and then PFA was quenched with 5 % BSA in 1 x PBS and 20 mM glycine for 30 min. Cells
720 were hybridized with probes as described above. This method was applied for the results
721 shown in Fig. 8C, E, Fig. 9, SFig. 8F-H.

722

723

724

725

726

727

728

729

730

731

732 **4. Immunofluorescence**

733 **4.1. Antibodies used**

Antibodies	Source	host	fixation	dilution	Identifier	internal Lab ID
monoclonal NPC (Mab414)	Abcam	mouse	MeOH	1:1000 (U2OS) or 1:2000 (HeLa)	ab24609	AB324
Lap2β	BD transduction laboratories	mouse	formaldehyde	1:500	611000; 27/LAP2	AB273
polyclonal Emerin	Abcam	rabbit	formaldehyde	1:500	ab40688	AB286AB321
serum LEM4	Ian Mattaj, (Asencio et al., 2012)	rabbit	formaldehyde	1:1000	BCFED3 20.1.10	AB282
polyclonal LBR	abcam	rabbit	MeOH		ab122919	AB264
serum ELYS/MEL-28	Iain Mattaj (Franz et al., 2007)	rabbit	formaldehyde	1:200	N/A	AB304
IgG, Alexa-Fluor™ 647	ThermoFischer Scientific	mouse	-	1:500	A21236	AB251
IgG, Alexa-Fluor™ 594	ThermoFischer Scientific	mouse	-	1:500	A11032	AB250
IgG, Alexa-Fluor™ 647	ThermoFischer Scientific	rabbit	-	1:500	A21245	AB316
IgG, Alexa-Fluor™ 594	ThermoFischer Scientific	rabbit	-	1:500	A11037	N/A
IgG, Alexa-Fluor™ 488	ThermoFischer Scientific	rabbit	-	1:500	A11034	AB252

734

735 **4.2 Immunofluorescence staining**

736 Cells in Fig. 3B were fixed 30 hours after pLacO transfection. Cells were either fixed with
737 methanol at -20 °C for 6 min, or with 1 % or 4 % paraformaldehyde for 10 min at RT. Cells
738 were permeabilized for 5 min or 10 min with 0.2 % or 0.1 % TritonX-100 at RT. Blocking was
739 performed with 5 % Bovine serum albumin (Boehringer Mannheim, now Roche) in 1x PBST
740 (1x PBS with 0.05 % Tween-20) for 1 hour at RT. Cells were then incubated with primary
741 antibodies diluted in blocking buffer for 1 hour. Followed by incubation with secondary
742 antibodies diluted in blocking buffer for 45 min to 1 hour. Cells were then stained with 2 µM
743 Hoechst33342 (Molecular probes, Thermo Fisher Scientific) for 10 min and mounted in Mowiol
744 with 1.4 % w/v DABCO. Cover slips were sealed with Nail polish (Lucerna Chem AG; Luzern,
745 Switzerland) and stored at 4 °C.

746

747 **5. Image acquisition**

748 Imaging was done at the Scientific Center for Optical and Electron Microscopy (ScopeM, ETH
749 Zurich).

750

751 **5.1. Fixed cell imaging**

752 For images of fixed cells, z-stacks minimally encompassing entire cells were acquired in 0.3
753 μm or 0.2 μm steps using a 60x NA 1.42 objective on a DeltaVision personalDV multiplexed
754 system (epifluorescence based IX71 (inverse) microscope; Olympus; Tokio, Japan) equipped
755 with a CoolSNAP HQ camera (Roper Scientific; Planegg, Germany).

756 Results shown in Fig. 7, SFig. 7 employed imaging using the DeltaVision personalDV
757 multiplexed system with a 60 x 1.42NA DIC Oil PlanApo Objective and a pco.edge 5.5 camera.
758 Z-stacks were acquired with 0.3 μm steps.

759 A Nikon Wide Field microscope (Nikon Ti2-E; Nikon, Tokio, Japan) was used in Fig. 1A-D,
760 SFig. 1, SFig. 2, SFig. 3 with the S Fluor 20x NA 0.75 DIC N2 WD 1.0mm. For Fig. 6 and SFig.
761 6F, Plan Apo lambda 60x NA 1.4 oil WD 0.13mm was used. Z-stacks with 41 slices x 0.3 μm
762 (12 mm total) were acquired, Dapi (Hoechst, DNA) channel was used as reference and the
763 chromatic offset in mCherry and GFP channels was corrected for.

764

765 **5.2. Live-cell microscopy**

766 For live-cell microscopy, three cell lines were used: Control HeLa, HeLa-Lacl, or HeLa K cells
767 stably expressing aa 244–453 of Lap2 β -GFP transiently overexpressing Lacl-mcherry.

768 For results displayed in Fig. 1E, F, Fig. 2A, B, Fig. 3C, Fig. 5, SFig. 4 cells were seeded on
769 Lab-Tek II chambers (Nunc, Thermo Scientific) with CO₂-independent media (Gibco)
770 containing 10 % FCS and incubated at a 37 °C on a Spinning Disk microscope (Nipkow
771 spinning disk setup with Nikon Eclipse T1 (inverse) microscope, equipped with 2x EMCCD
772 Andor iXon Ultra cameras, LUDL BioPrecision2 stage with Piezo Focus, Carl Zeiss
773 Microscopy; Jena, Germany). For imaging in Fig. 5 the GFP-Like (Em 520/35) and DsRed-like
774 (Em 617/73) Emission Filter Wheels and 2x Evolve 512 cameras (Photometrics; Tucson,
775 Arizona, United States) were used. For long-term time-lapse imaging (Fig. 5, SFig. 4), cells
776 were recorded every 15 min in z-stacks (33x 0.7 μm steps using a 63x 1.2 NA objective). To
777 monitor cell contours, cells were illuminated with transmission light with single z-focus. For
778 some still images cells expressing Sec61-mCherry (Fig. 2A), eGFP-KDEL (Fig. 2B) and eGFP-
779 BAF (Fig. 3C) were imaged after incubation with 2 μM Hoechst33342 for 10 min, using a
780 DeltaVision microscope (DeltaVision personalDV system (epifluorescence based IX71
781 (inverse) microscope; Olympus)).

782 For results displayed in Fig. 1, SFig. 2, SFig. 3, HeLa Control cells were seeded on ibidi 8-well
783 chambers (ibidi μ -Slide 8 well ibiTreat, Gräfelfing, Germany). 24 hours after seeding, cells
784 were incubated at 37 °C with 5% CO₂ (OkoLab, Pozzouli NA, Italy) either at the Visitron
785 Spinning Disk (experiments e1 (internal Lab ID: EXP345) and e2 (internal Lab ID: EXP337))
786 or a Nikon Wide Field microscope (Nikon Ti2-E (inverse), experiments e3 and e4 (internal Lab
787 ID: EXP604)). For Visitron spinning disk imaging a GFP-Like (Em 520/35) Emission Filter

788 Wheel and 2x Evolve 512 cameras (Photometrics) were used. Bright field imaging was done
789 with the coolLED pE-100 control system (coolLED; Andover, Great Britain). For Nikon Wide
790 Field imaging the GFP (Em 515/30) Emission Filter Wheel or bright field pre-setting was used.
791 For detection, the Orca Fusion BT (Hamamatsu; Shizuoka, Japan) (2304x2304 pixels, 6.5 μ m
792 x 6.5 μ m) system was used. For each experiment at the Visitron Spinning Disk microscope, 5
793 regions of interest (ROI) were imaged. For each experiment at the Nikon Wide Field
794 microscope, 6 ROI were imaged. In the live-cell analysis included are only ROI with 0.9766
795 cells/pixel, thus one ROI of e1 at the Visitron Spinning Disk microscope and two ROI of e3 as
796 well as two ROI of e4 at the Nikon Wide Field microscope were excluded. Cells were recorded
797 every 30 min as z-stacks (22 x 0.7 μ m steps using 20x 0.75 CFI Plan Apo VC at the Visitron
798 Spinning disk and 22 x 0.7 μ m steps using S Fluor 20 x NA 0.75 DIC N2 WD 1.0mm at the
799 Nikon Wide Field). On both microscopes, cells were lipofected with pLacO using X-
800 tremeGENE 9 DNA Transfection Reagent (Roche). The plasmid:transfection reagent ratio
801 (w:v) was 1:3 with a plasmid DNA concentration of 100 ng/cm². The lipofection mix remained
802 on the cells during imaging. The death rate was low at both microscopes (SFig. 2A).

803

804 **5.3. FRAP**

805 FRAP experiments (Fig. 4E-G) were performed using a modified method that was previously
806 reported (Clay et al., 2014). 24 hours after pLacO transfection, live HeLa-LacI cells (seeded
807 on a Lab-TekTM II chamber, CO₂-independent media, 37 °C incubator) and free eGFP were
808 imaged on a confocal microscope (LSM 760; Carl Zeiss Microscopy) with a Plan Apochromat
809 63x /1.4 NA oil immersion objective. The ZEN software (Carl Zeiss Microscopy) was used to
810 control the microscope. eGFP emission was detected with a 505 nm long pass filter.
811 Photobleaching was applied on a region of interest (cluster and then control area) as indicated
812 in Fig. 4E-G. Bleaching was applied with 50-100 iterations using 30-50 % laser power, but
813 always with the same settings between the cluster and control area in each cell.

814

815 **5.4. Correlative light and electron microscopy (CLEM)**

816 HeLa K cells stably expressing LacI-NLS-mCherry were cultured on a 3.5 cm glass bottom
817 dish with grid (MatTek; Ashland, Massachusetts, United States) and transfected with pLacO
818 for 24 hours. Cells were processed as described in (Wang et al., 2016).

819

820 **6. Data Analysis (Fiji, Prism, Diatrack, etc.)**

821 **6.1. Image processing**

822 Images acquired from DeltaVision (Olympus) microscope (Fig. 2C, Fig. 3B-D, Fig. 4A-D, Fig.
823 8, SFig. 9A, SFig. 5A, E, SFig. 6A, SFig. 7C, D, SFig. 8A, B, D) were deconvolved using
824 Softworx (Applied Precision; Rača, Slovakia). Images acquired from LSM 710 confocal

825 microscope were deconvolved using Huygens Software (Scientific Volume Imaging;
826 Hilversum, Netherlands) before correlating with EM images (Fig. 2A). The correlation analysis
827 between confocal and EM images (Fig. 3A) were performed using Amira software
828 (FEI/Thermo Fisher Scientific), as in (Wang et al., 2016). General, the presented images are
829 single z-slices or if indicated projections of multiple z-slices images.
830 Images in Fig. 3A (confocal image), Fig. 6 and SFig. 6F were deconvolved using Huygens
831 (Scientific Volume Imaging).

832

833 **6.2. Image analyses**

834 Images were analyzed using Fiji 1.51n Software.

835

836 **6.2.1 Colocalization**

837 For co-localization analyses, the overlay of the reporter fluorescence and LacI fluorescence
838 was used (Fig. 2C, Fig. 6, Fig. 8, SFig. 6D, E, SFig. 8). The qualitative classes for reporter
839 molecules “enriched”, “non-enriched”, “present” and “absent” are established applying the
840 following rules:

841

842 For experiments presented in Fig. 3, Fig. 4:

843 Generally, marker fluorescence intensities were used to qualitatively determine co-localization
844 of markers with the plasmid focus with the following criteria.

845 “Non-enriched”: plasmid foci with marker fluorescence signal in the z-stack slice in, directly
846 underneath or above the position of the plasmid focus, and/or marker fluorescence signal in
847 xy-direction adjacent. The intensity of the marker fluorescence is like the cytoplasmic marker
848 fluorescence (relative readout to the intensity of the rest of the cell).

849 Plasmid foci with marker “enriched” have marker fluorescence at same positions described in
850 “non-enriched”, but with higher intensities compared to the reference marker fluorescence of
851 the respective marker (i.e., Emerin at NE or in ER; LEM4 in ER). Where sensible, results state
852 the two “enriched” reference marker fluorescence (i.e., ER or NE).

853 Category “present” (Fig. 8 and Fig. 4) encompasses “enriched” and “non-enriched”.

854 Plasmid foci with marker “absent” do not have marker fluorescence in the adjacent slides,
855 underneath or above the position of the focus, nor a marker fluorescence signal in xy direction
856 adjacent to the focus nor in the sliced with the focus.

857 For data presented in Fig. 3E:

858 For Emerin and Lap2 β , the quantitative enrichment factor analysis (below) were back
859 translated into qualitative classification: “enriched” with an enrichment factor >1 , or “non-
860 enriched” with $0 > \text{enrichment factor} > 1$, or “absent” for enrichment factor being zero. For BAF

861 and LBR, the classification of “enriched”, “non-enriched”, and “absent” as described above for
862 Fig. 3 was used.

863

864 For data presented in Fig. 6, SFig. 6C-F:

865 In the single z-slice, where the plasmid focus was in focus, a line scan across the biggest axis
866 of the plasmid focus and either the ER (for LEM4) or across the nucleus (for Emerin) was
867 made, displaying the intensity distribution along that line (Fiji, line scan). Classification was
868 according to the following intensity criteria: enriched > NE or > ER: the average intensity of
869 the reporter (Emerin or LEM4) at the plasmid focus was higher compared to the average
870 reporter intensity at the NE or surrounding ER, displayed along the line. Like ER: fluorescence
871 of the reporter (Emerin or LEM4) was in average identical the intensity in the ER surrounding
872 the plasmid focus. Absent: no intensity of the reporter (Emerin or LEM4) at the plasmid focus.

873

874 For the experiments presented in Fig. 7:

875 Intensities of reporter proteins (LEM4 or Emerin) at the plasmid focus were visually compared
876 to intensities reporter proteins in the surrounding cytoplasm. “Present”: If the reporter intensity
877 was equal or higher at the plasmid focus than that of the surrounding cytoplasm in the focal
878 slice, directly underneath or above the focus-position of the plasmid focus (0.3 μm distances).
879 Otherwise, the classification was “absent”.

880

881 For the experiments presented in SFig. 7B, C:

882 The intensity of Emerin immunofluorescence was measured as RawIntDen (Fiji) in a square
883 (20x20 px) covering ER and in a same sized square covering the nucleus of a single cells in
884 maximum intensity projected images. Chosen were in both cases regions where the intensity
885 appeared the most intense as judge by eye. The ratio between the RawIntDen value at the
886 NE divided by that at the ER was calculated for each cell with minimally 1 cytoplasmic plasmid
887 focus. A ratio above 1 reports about a higher intensity of Emerin (and therefore more Emerin)
888 at the NE compared to the ER of that same cell. A ratio below 1 represents a higher intensity
889 of Emerin (and therefore more Emerin) at the ER compared to the NE of the same cell.

890

891 Quantitative enrichment factor analysis (SFIG. 6B):

892 Single z-slice images were analyzed. The fluorescence intensity was measured along a line
893 crossing the plasmid focus and the nucleus. Along this line, the fluorescent intensities of two
894 brightest pixels at the edges of the plasmid focus ($I(c1), I(c2)$) or the nucleus ($I(n1), I(n2)$),
895 were averaged. Another averaged intensity of 30-50 pixels along this line, in a cytoplasmic
896 region, was used as background intensity ($I(\text{background})$). The enrichment factor was

897 calculated as: (Enrichment factor = $((I(c1)+I(c2))*0.5 - I(\text{background}))/((I(n1)+I(n2))*0.5 - I(\text{background}))$).

899

900 **6.2.2 Live-cell imaging analyses**

901 **Plasmid focus localization** (Fig. 1, SFig. 2, SFig. 3):

902 For plasmid focus analyses, two interphase localizations are classified: cytoplasmic and
903 nuclear. Cytoplasmic plasmid foci: These intracellular LacI-positive plasmid foci are outside of
904 the volume marked by LacI-NLS-GFP fluorescence reporting about the nucleus or are at the
905 cytoplasmic side of the nuclear envelope, which is reported by the outer boarder of the nuclear
906 LacI-NLS-GFP fluorescence, but with minimally 1 pixel of background intensity between the
907 LacI intensity at the plasmid focus and that of the nucleus. Plasmid foci in the nucleus are
908 either nucleoplasmic LacI-positive foci or LacI-positive foci at the nucleoplasmic side of the
909 nuclear envelope, which is reported by the outer boarder of nuclear LacI-NLS-GFP
910 fluorescence. Nucleoplasmic plasmid foci (nuclear foci) are defined as plasmid foci inside the
911 volume of nuclear LacI-NLS-GFP fluorescence but with an intensity higher than that of the
912 general nuclear LacI-NLS-GFP fluorescence. In addition, the z-slice in which the plasmid focus
913 is most in focus (focal-z-slice) and at highest intensity is also the z-slice, in which nuclear LacI-
914 NLS-GFP fluorescence covers the biggest area. Further, the focal-z-slice of the plasmid lies
915 in between other z-slices in which the general nuclear LacI-NLS-GFP fluorescence is still in
916 focus. Typically, depending on the z-stack spacing, the general nuclear LacI-NLS-GFP
917 fluorescence is still in focus within +/- 1 μm of the focal plane of the plasmid focus. This is to
918 be compared to a situation, where a plasmid focus is at the nuclear envelope and thus in an
919 upper z-slice. In this case the plasmid focal plane is not identical with the z-slice of the biggest
920 area of general nuclear fluorescence. These classification criteria were used in Fig. 1, SFig.
921 2, SFig. 3 as well as for classification of plasmid foci being formed in the nucleoplasm in SFig.
922 5G+H. We chose these strict conditions to exclude the option of a false positive nuclear
923 assignment to plasmid foci.

924

925 **Origin-destination analysis** (Fig. 1D, SFig. 2H):

926 To avoid analyzing plasmid foci that formed in the cytoplasm but in close proximity to the NE,
927 we excluded plasmid foci that formed at the inner side of the nuclear periphery from the
928 analysis focusing thus on foci formed in the inner nucleoplasm. To allow for sorting time the
929 last 25 % of the forming plasmid foci in the pooled data set were excluded from this analysis.
930 For the “origin-destination” analysis the location of formation of each plasmid focus was noted
931 (“origin”) (either interphase: cytoplasm or nucleoplasm, or during mitosis). Then, after tracing
932 the focus over time until the end of imaging, the location of each plasmid focus at imaging end
933 (“destination”) was noted. If during imaging a cell fused with another cell, died, produced a

934 micronucleus, the nucleus fragmented, the plasmid focus disappeared, or the cell was in
935 mitosis at the end of imaging the focus localization in the last frame before one of these events
936 was noted as the corresponding destination of the given plasmid focus. Only cells that
937 completed a mitosis (first frame with two distinct nuclei in LacI-NLS-GFP channel and two fully
938 divided cells in brightfield channel) were analyzed.

939

940 **FRAP quantification** (Fig. 4E, F):

941 Using Fiji, the mean fluorescence recovery signal was quantified in the bleached area. The
942 fluorescence signal was normalized to that at the beginning of the experiment. All experiments
943 were transferred to Prism software (GraphPad) and fit on an exponential FRAP curve, the
944 mobile fraction was measured by determining the half time ($t_{1/2}$) of fluorescence recovery to
945 reach a plateau level.

946

947 **FISH co-localization analysis** (Fig. 8, Fig. 9, SFig. 8):

948 Fluorescence signals of stained proteins were boosted until the background level of the cell's
949 cytoplasm was visible. Proteins co-localized at telomeric DNA if the signals at the telomeric
950 DNA foci were visually than the background in close vicinity and the boosted setting.

951

952 **7. Statistics**

953 Statistics were conducted using Prism 8.0.0 (GraphPad) built-in analysis tools, methods used
954 are indicated in the figure legends.

955 Data were tested with Gaussian distribution for normality (*D'Agostino & Pearson* normality test)
956 ($\alpha=0.05$) if t-tests were used.

957

958 **Acknowledgements**

959 We thank Yves Barral (ETH-Zürich), for continued discussions and support of this study. We
960 thank Madhav Jagannathan, members of the Kroschewski and Barral labs for helpful
961 discussions and comments on the manuscript. We acknowledge financial support by Swiss
962 National Science Foundation (grant 31003A_172908/1 to RK) and the Novartis foundation for
963 medical-biological research (grant 20C229 to RK).

964

965 **Competing interest**

966 The authors declare no conflict of interest

967

968

969

970

971 **References**

972

973 Anderson, D.J., and M.W. Hetzer. 2007. Nuclear envelope formation by chromatin-mediated
974 reorganization of the endoplasmic reticulum. *Nature Cell Biology*. 9:1160-1166.

975 Anderson, D.J., and M.W. Hetzer. 2008. Reshaping of the endoplasmic reticulum limits the
976 rate for nuclear envelope formation. *The Journal of Cell Biology*. 182:911-924.

977 Asencio, C., I.F. Davidson, R. Santarella-Mellwig, T.B.N. Ly-Hartig, M. Mall, M.R. Wallenfang,
978 I.W. Mattaj, and M. Gorjánácz. 2012. Coordination of kinase and phosphatase
979 activities by Lem4 enables nuclear envelope reassembly during mitosis. *Cell*. 150:122
980 - 135.

981 Beaudouin, J., D. Gerlich, N. Daigle, R. Eils, and J. Ellenberg. 2002. Nuclear Envelope
982 Breakdown Proceeds by Microtubule-Induced Tearing of the Lamina. *Cell*. 108:83-96.

983 Buchwalter, A., R. Schulte, H. Tsai, J. Capitanio, and M. Hetzer. 2019. Selective clearance of
984 the inner nuclear membrane protein emerin by vesicular transport during ER stress.
985 *eLife*. 8.

986 Cesare, A.J., and J.D. Griffith. 2004. Telomeric DNA in ALT cells is characterized by free
987 telomeric circles and heterogeneous t-loops. *Molecular and cellular biology*. 24:9948 -
988 9957.

989 Chen, T., T.L. Muratore, C.E. Schaner-Tooley, J. Shabanowitz, D.F. Hunt, and I.G. Macara.
990 2007. N-terminal α -methylation of RCC1 is necessary for stable chromatin association
991 and normal mitosis. *Nature Cell Biology*. 9:596 - 603.

992 Chen, Y.-A., Y.-L. Shen, H.-Y. Hsia, Y.-P. Tiang, T.-L. Sung, and L.-Y. Chen. 2017.
993 Extrachromosomal telomere repeat DNA is linked to ALT development via cGAS-
994 STING DNA sensing pathway. *Nat Struct Mol Biol*. 24:1124-1131.

995 Clay, L., F. Caudron, A. Denoth-Lippuner, B. Boettcher, S. Buvelot Frei, E.L. Snapp, and Y.
996 Barral. 2014. A sphingolipid-dependent diffusion barrier confines ER stress to the
997 yeast mother cell. *eLife*. 3:e01883.

998 Crasta, K., N.J. Ganem, R. Dagher, A.B. Lantermann, E.V. Ivanova, Y. Pan, L. Nezi, A.
999 Protopopov, D. Chowdhury, and D. Pellman. 2012. DNA breaks and chromosome
1000 pulverization from errors in mitosis. *Nature*. 482:53-58.

1001 Denoth-Lippuner, A., M.K. Krzyzanowski, C. Stober, and Y. Barral. 2014. Role of SAGA in the
1002 asymmetric segregation of DNA circles during yeast ageing. *eLife*. 3:e03790.

1003 Ferrandiz, N., L. Downie, G.P. Starling, and S.J. Royle. 2022. Endomembranes promote
1004 chromosome missegregation by ensheathing misaligned chromosomes. *Journal of
1005 Cell Biology*. 221:e202203021.

1006 Franz, C., R. Walczak, S. Yavuz, R. Santarella, M. Gentzel, P. Askjaer, V. Galy, M. Hetzer,
1007 I.W. Mattaj, and W. Antonin. 2007. MEL-28/ELYS is required for the recruitment of
1008 nucleoporins to chromatin and postmitotic nuclear pore complex assembly. *EMBO
1009 Reports*. 8:165 - 172.

1010 Gerber, T., C. Loureiro, N. Schramma, S. Chen, A. Jain, A. Weber, A. Weigert, M. Santel, K.
1011 Alim, B. Treutlein, and J.G. Camp. 2022. Spatial transcriptomic and single-nucleus
1012 analysis reveals heterogeneity in a gigantic single-celled syncytium. *eLife*. 11:e69745.

1013 Gómez-Saldivar, G., A. Fernandez, Y. Hirano, M. Mauro, A. Lai, C. Ayuso, T. Haraguchi, Y.
1014 Hiraoka, F. Piano, and P. Askjaer. 2016. Identification of Conserved MEL-28/ELYS
1015 Domains with Essential Roles in Nuclear Assembly and Chromosome Segregation.
1016 *PLoS genetics*. 12:e1006131.

1017 Grandjean, M., P.-A. Girod, D. Calabrese, K. Kostyrko, M. Wicht, F. Yerly, C. Mazza, J.S.
1018 Beckmann, D. Martinet, and N. Mermod. 2011. High-level transgene expression by
1019 homologous recombination-mediated gene transfer. *Nucleic Acids Research*.
1020 39:e104-e104.

1021 Greseth, M.D., and P. Traktman. 2022. The Life Cycle of the Vaccinia Virus Genome. *Annual
1022 Review of Virology*. 9:239-259.

1023 Guey, B., M. Wischnewski, A. Decout, K. Makasheva, M. Kaynak, M.S. Sakar, B. Fierz, and
1024 A. Ablasser. 2020. BAF restricts cGAS on nuclear DNA to prevent innate immune
1025 activation. *Science (New York, NY)*. 369:823 - 828.

1026 Güttinger, S., E. Laurell, and U. Kutay. 2009. Orchestrating nuclear envelope disassembly and
1027 reassembly during mitosis. *Nature Reviews Molecular Cell Biology*. 10:178-191.

1028 Haraguchi, T., T. Kojidani, T. Koujin, T. Shimi, H. Osakada, C. Mori, A. Yamamoto, and Y.
1029 Hiraoka. 2008. Live cell imaging and electron microscopy reveal dynamic processes
1030 of BAF-directed nuclear envelope assembly. *Journal of Cell Science*. 121:2540-2554.

1031 Haraguchi, T., T. Koujin, T. Hayakawa, T. Kaneda, C. Tsutsumi, N. Imamoto, C. Akazawa, J.
1032 Sukegawa, Y. Yoneda, and Y. Hiraoka. 2000. Live fluorescence imaging reveals early
1033 recruitment of emerin, LBR, RanBP2, and Nup153 to reforming functional nuclear
1034 envelopes. *Journal of Cell Science*. 113:779-794.

1035 Haraguchi, T., T. Koujin, M. Segura-Totten, K.K. Lee, Y. Matsuoka, Y. Yoneda, K.L. Wilson,
1036 and Y. Hiraoka. 2001. BAF is required for emerin assembly into the reforming nuclear
1037 envelope. *Journal of Cell Science*. 114:4575-4585.

1038 Haraguchi, T., T. Koujin, T. Shindo, S. Bilir, H. Osakada, K. Nishimura, Y. Hirano, H. Asakawa,
1039 C. Mori, S. Kobayashi, Y. Okada, Y. Chikashige, T. Fukagawa, S. Shibata, and Y.
1040 Hiraoka. 2022. Transfected plasmid DNA is incorporated into the nucleus via nuclear
1041 envelope reformation at telophase. *Communications Biology*. 5:78.

1042 Hatch, Emily M., Andrew H. Fischer, Thomas J. Deerinck, and Martin W. Hetzer. 2013.
1043 Catastrophic Nuclear Envelope Collapse in Cancer Cell Micronuclei. *Cell*. 154:47-60.

1044 Ibrahim, N., A. Wicklund, and M.S. Wiebe. 2011. Molecular characterization of the host
1045 defense activity of the barrier to autointegration factor against vaccinia virus. *Journal
1046 of virology*. 85:11588–11600.

1047 Karg, T., B. Warecki, and W. Sullivan. 2015. Aurora B-mediated localized delays in nuclear
1048 envelope formation facilitate inclusion of late-segregating chromosome fragments.
1049 *Molecular Biology of the Cell*. 26:2227-2241.

1050 Kneissig, M., K. Keuper, M.S.d. Pagter, M.J.v. Roosmalen, J. Martin, H. Otto, V. Passerini,
1051 A.C. Sparr, I. Renkens, F. Kropveld, A. Vasudevan, J.M. Sheltzer, W.P. Kloosterman,
1052 and Z. Storchova. 2019. Micronuclei-based model system reveals functional
1053 consequences of chromothripsis in human cells. *eLife*. 8:e50292.

1054 Kobayashi, S., T. Koujin, T. Kojidani, H. Osakada, C. Mori, Y. Hiraoka, and T. Haraguchi. 2015.
1055 BAF is a cytosolic DNA sensor that leads to exogenous DNA avoiding autophagy.
1056 *Proceedings of the National Academy of Sciences of the United States of America*.
1057 112:7027–7032.

1058 Kopecky, P., K. Tiedemann, D. Alkekhaia, C. Zechner, B. Millard, B. Schoeberl, and S.V.
1059 Komarova. 2014. Autocrine signaling is a key regulatory element during
1060 osteoclastogenesis. *Biology Open*. 3:767-776.

1061 Kutay, U., R. Jühlen, and W. Antonin. 2021. Mitotic disassembly and reassembly of nuclear
1062 pore complexes. *Trends in Cell Biology*. 31:1019-1033.

1063 Langereis, M.A., H.H. Rabouw, M. Holwerda, L.J. Visser, and F.J.M.v. Kuppeveld. 2015.
1064 Knockout of cGAS and STING Rescues Virus Infection of Plasmid DNA-Transfected
1065 Cells. *Journal of virology*. 89:11169 - 11173.

1066 Lansdorp, P.M., N.P. Verwoerd, F.M.v.d. Rijke, V. Dragowska, M.-T. Little, R.W. Dirks, A.K.
1067 Raap, and H.J. Tanke. 1996. Heterogeneity in Telomere Length of Human
1068 Chromosomes. *Human Molecular Genetics*. 5:685-691.

1069 Lee, K.K., T. Haraguchi, R.S. Lee, T. Koujin, Y. Hiraoka, and K.L. Wilson. 2001. Distinct
1070 functional domains in emerin bind lamin A and DNA-bridging protein BAF. *Journal of
1071 Cell Science*. 114:4567 - 4573.

1072 Lefebvre, M.D., and M.A. Valvano. 2002. Construction and Evaluation of Plasmid Vectors
1073 Optimized for Constitutive and Regulated Gene Expression in Burkholderia cepacia
1074 Complex Isolates. *Applied and Environmental Microbiology*. 68:5956-5964.

1075 Li, H.Y., D. Wirtz, and Y. Zheng. 2003. A mechanism of coupling RCC1 mobility to RanGTP
1076 production on the chromatin in vivo. *Journal of Cell Biology*. 160:635-644.

1077 Liu, S., M. Kwon, M. Mannino, N. Yang, F. Renda, A. Khodjakov, and D. Pellman. 2018.
1078 Nuclear envelope assembly defects link mitotic errors to chromothripsis. *Nature*.
1079 561:551-555.

1080 Lu, L., M.S. Ladinsky, and T. Kirchhausen. 2009. Cisternal organization of the endoplasmic
1081 reticulum during mitosis. *Molecular Biology of the Cell*. 20:3471 - 3480.

1082 Ludtke, J.J., M.G. Sebestyén, and J.A. Wolff. 2002. The Effect of Cell Division on the Cellular
1083 Dynamics of Microinjected DNA and Dextran. *Molecular Therapy*. 5:579-588.

1084 Mimura, Y., M. Takagi, M. Clever, and N. Imamoto. 2016. ELYS regulates the localization of
1085 LBR by modulating its phosphorylation state. *Journal of Cell Science*. 129:4200-4212.

1086 Mühlhäuser, P., and U. Kutay. 2007. An in vitro nuclear disassembly system reveals a role
1087 for the RanGTPase system and microtubule-dependent steps in nuclear envelope
1088 breakdown. *The Journal of Cell Biology*. 178:595 - 610.

1089 Mutsafi, Y., E. Shiloni, A. Shimon, and A. Minsky. 2013. Membrane Assembly during the
1090 Infection Cycle of the Giant Mimivirus. *Plos Pathog*. 9:e1003367.

1091 Nakano, M., S. Cardinale, V.N. Noskov, R. Gassmann, P. Vagnarelli, S. Kandels-Lewis, V.
1092 Larionov, W.C. Earnshaw, and H. Masumoto. 2008. Inactivation of a Human
1093 Kinetochore by Specific Targeting of Chromatin Modifiers. *Developmental Cell*. 14:507
1094 - 522.

1095 Noer, J.B., O.K. Hørsdal, X. Xiang, Y. Luo, and B. Regenberg. 2022. Extrachromosomal
1096 circular DNA in cancer: history, current knowledge, and methods. *Trends in Genetics*.
1097 38:766-781.

1098 Orr, B., F.D. Sousa, A.M. Gomes, O. Afonso, L.T. Ferreira, A.C. Figueiredo, and H. Maiato.
1099 2021. An anaphase surveillance mechanism prevents micronuclei formation from
1100 frequent chromosome segregation errors. *Cell Reports*. 37:109783.

1101 Otsuka, S., A.M. Steyer, M. Schorb, J.-K. Hériché, M.J. Hossain, S. Sethi, M. Kueblbeck, Y.
1102 Schwab, M. Beck, and J. Ellenberg. 2018. Postmitotic nuclear pore assembly proceeds
1103 by radial dilation of small membrane openings. *Nat Struct Mol Biol*. 25:21-28.

1104 Otsuka, S., J.O.B. Tempkin, W. Zhang, A.Z. Politi, A. Rybina, M.J. Hossain, M. Kueblbeck, A.
1105 Callegari, B. Koch, N.R. Morero, A. Sali, and J. Ellenberg. 2023. A quantitative map of
1106 nuclear pore assembly reveals two distinct mechanisms. *Nature*. 613:575-581.

1107 Paulsen, T., P. Kumar, M.M. Koseoglu, and A. Dutta. 2018. Discoveries of Extrachromosomal
1108 Circles of DNA in Normal and Tumor Cells. *Trends in Genetics*. 34:270 - 278.

1109 Rasala, B.A., A.V. Orjalo, Z. Shen, S. Briggs, and D.J. Forbes. 2006. ELYS is a dual
1110 nucleoporin/kinetochore protein required for nuclear pore assembly and proper cell
1111 division. *Proceedings of the National Academy of Sciences of the United States of
1112 America*. 103:17801-17806.

1113 Regev, A., S. Cohen, E. Cohen, I. Bar-Am, and S. Lavi. 1999. Telomeric repeats on small
1114 polydisperse circular DNA (spcDNA) and genomic instability. *Oncogene*. 17:3455 -
1115 3461.

1116 Rohner, S., S.M. Gasser, and P. Meister. 2008. Modules for cloning-free chromatin tagging in
1117 *Saccharomyces cerevisiae*. *Yeast*. 25:235 - 239.

1118 Samwer, M., M.W.G. Schneider, R. Hoefler, P.S. Schmalhorst, J.G. Jude, J. Zuber, and D.W.
1119 Gerlich. 2017. DNA Cross-Bridging Shapes a Single Nucleus from a Set of Mitotic
1120 Chromosomes. *Cell*. 170:956 - 972.e923.

1121 Schellhaus, A.K., P. De Magistris, and W. Antonin. 2016. Nuclear Reformation at the End of
1122 Mitosis. *Journal of Molecular Biology*. 428:1962-1985.

1123 Schmitz, M.H.A., M. Held, V. Janssens, J.R.A. Hutchins, O. Hudecz, E. Ivanova, J. Goris, L.
1124 Trinkle-Mulcahy, A.I. Lamond, I. Poser, A.A. Hyman, K. Mechteder, J.-M. Peters, and
1125 D.W. Gerlich. 2010. Live-cell imaging RNAi screen identifies PP2A-B55α and importin-
1126 β1 as key mitotic exit regulators in human cells. *Nature Cell Biology*. 12:886-893.

1127 Shcheprova, Z., S. Baldi, S.B. Frei, G. Gonnet, and Y. Barral. 2008. A mechanism for
1128 asymmetric segregation of age during yeast budding. *Nature*. 454:728-734.

1129 Shimi, T., T. Koujin, M. Segura-Totten, K.L. Wilson, T. Haraguchi, and Y. Hiraoka. 2004.
1130 Dynamic interaction between BAF and emerin revealed by FRAP, FLIP, and FRET
1131 analyses in living HeLa cells. *Journal of Structural Biology*. 147:31 - 41.

1132 Shimizu, N., N. Itho, H. Utiyama, and G.M. Wahl. 1998. Selective Entrapment of
1133 Extrachromosomally Amplified DNA by Nuclear Budding and Micronucleation during S
1134 Phase. *The Journal of Cell Biology*. 140:1307 - 1320.

1135 Shimizu, N., F. Kamezaki, and S. Shigematsu. 2005. Tracking of microinjected DNA in live
1136 cells reveals the intracellular behavior and elimination of extrachromosomal genetic
1137 material. *Nucleic Acids Research*. 33:6296 - 6307.

1138 Tokutake, Y., T. Matsumoto, T. Watanabe, S. Maeda, H. Tahara, S. Sakamoto, H. Niida, M.
1139 Sugimoto, T. Ide, and Y. Furuichi. 1998. Extra-Chromosomal Telomere Repeat DNA
1140 in Telomerase-Negative Immortalized Cell Lines. *Biochem Biophys Res Commun*.
1141 247:765-772.

1142 Ulbert, S., M. Platani, S. Boue, and I.W. Mattaj. 2006. Direct membrane protein-DNA
1143 interactions required early in nuclear envelope assembly. *Journal of Cell Biology*.
1144 173:469-476.

1145 Ventimiglia, L.N., M.A. Cuesta-Geijo, N. Martinelli, A. Caballe, P. Macheboeuf, N. Miguet, I.M.
1146 Parnham, Y. Olmos, J.G. Carlton, W. Weissenhorn, and J. Martin-Serrano. 2018.
1147 CC2D1B Coordinates ESCRT-III Activity during the Mitotic Reformation of the Nuclear
1148 Envelope. *Developmental Cell*. 47:547-563.e546.

1149 Vidaček, N.Š., A. Ćukušić, M. Ivanković, H. Fulgosi, M. Huzak, J.R. Smith, and I. Rubelj. 2010.
1150 Abrupt telomere shortening in normal human fibroblasts. *Experimental Gerontology*.
1151 45:235-242.

1152 Walther, T.C., P. Askjaer, M. Gentzel, A. Habermann, G. Griffiths, M. Wilm, I.W. Mattaj, and
1153 M. Hetzer. 2003. RanGTP mediates nuclear pore complex assembly. *Nature*. 424:689
1154 - 694.

1155 Wang, R.C., A. Smogorzewska, and T. de Lange. 2004. Homologous Recombination
1156 Generates T-Loop-Sized Deletions at Human Telomeres. *Cell*. 119:355-368.

1157 Wang, X., N. Le, A. Denoth-Lippuner, Y. Barral, and R. Kroschewski. 2016. Asymmetric
1158 partitioning of transfected DNA during mammalian cell division. *Proceedings of the
1159 National Academy of Sciences of the United States of America*. 113:7177-7182.

1160 Warecki, B., X. Ling, I. Bast, and W. Sullivan. 2020. ESCRT-III-mediated membrane fusion
1161 drives chromosome fragments through nuclear envelope channels. *The Journal of Cell
1162 Biology*. 219:e201905091.

1163 Ye, Q., and H.J. Worman. 1996. Interaction between an Integral Protein of the Nuclear
1164 Envelope Inner Membrane and Human Chromodomain Proteins Homologous to
1165 Drosophila HP1*. *Journal of Biological Chemistry*. 271:14653-14656.

1166 Zhang, C.-Z., A. Spektor, H. Cornils, J.M. Francis, E.K. Jackson, S. Liu, M. Meyerson, and D.
1167 Pellman. 2015. Chromothripsis from DNA damage in micronuclei. *Nature*. 522:179 -
1168 184.

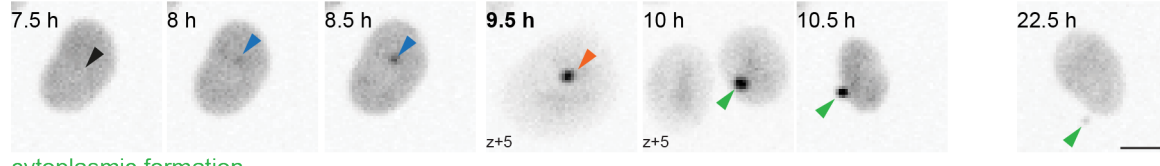
1169 Zheng, R., R. Ghirlando, M.S. Lee, K. Mizuuchi, M. Krause, and R. Craigie. 2000. Barrier-to-
1170 autointegration factor (BAF) bridges DNA in a discrete, higher-order nucleoprotein
1171 complex. *Proceedings of the National Academy of Sciences of the United States of
1172 America*. 97:8997 - 9002.

1173

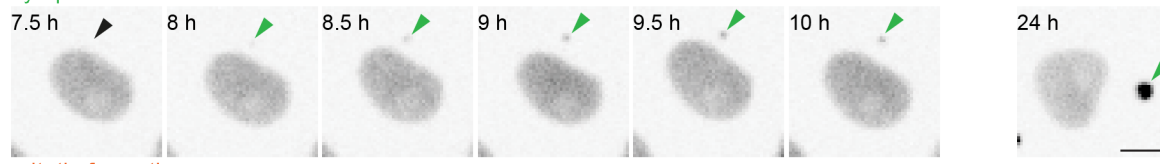
Fig. 1

A

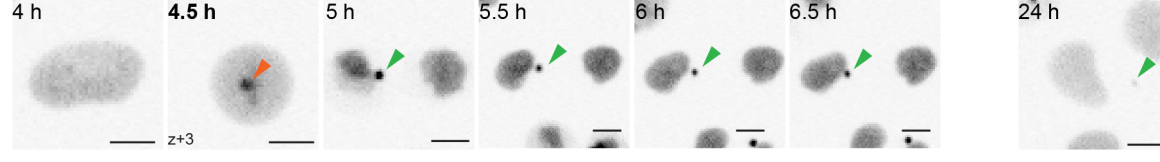
LacI
nucleoplasmic formation



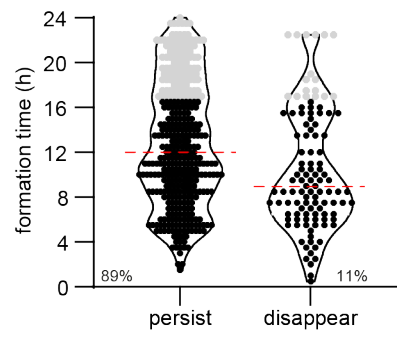
cytoplasmic formation



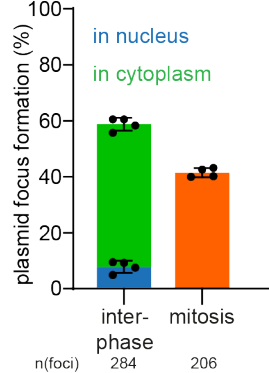
mitotic formation



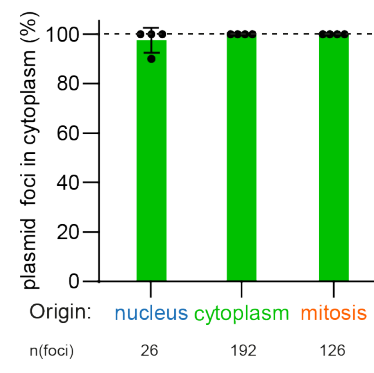
B



C

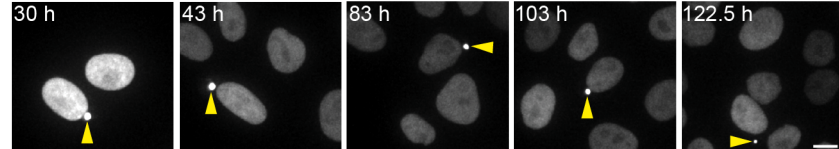


D

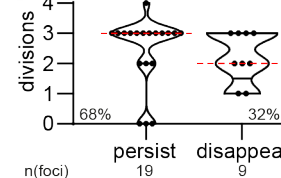


E

LacI



F

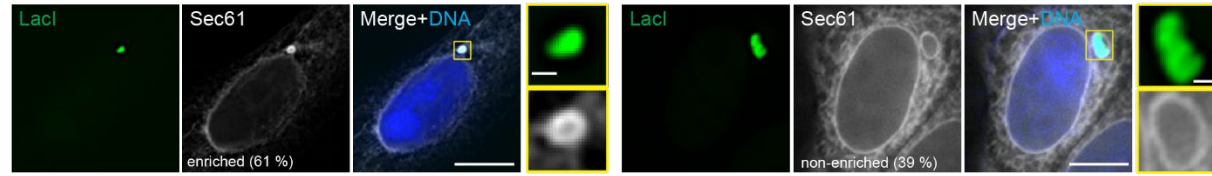


Cytoplasmic plasmid foci have 3 origins and are maintained in the cytoplasm long-term.

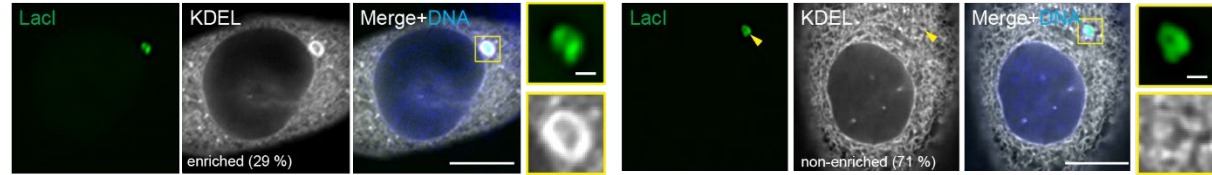
(A) Time-lapse images of focus formations in HeLa-LacI cells lipofected at imaging start with pLacO. Scale bar, 10 μ m. Time, after lipofection; bold time, mitosis. Arrowheads: nucleoplasmic focus, blue; cytoplasmic, green; mitosis, orange; future focus formation, black. Single z-slices. **(B)** Timing of individual focus formation events (circle) after pLacO lipofection. Persisting (persist) and disappearing (disappear) foci. 4 experiments (exp.) pooled; n(foci): 490; median, red. Last 25 % of all appearances, grey. % relative to all foci formed. **(C)** Focus formations in interphase or mitotic cells relative to all focus formations. 1 exp., circle; mean & SD. **(D)** Foci that are in the cytoplasm at imaging end depending on their origin. Last 25 % formations (in B) excluded. Color code as in (A). n(foci): 344; 100 % reference, dashed line. **(E, F)** Imaging started 30 hours after pLacO lipofection. 1 exp., n(cells): 28. **(E)** Time-lapse images of a pLacO transfected cell with one persisting focus, yellow arrowhead. Images, maximum intensity (max.) projected; **(F)** Maximal number of divisions a focus was detectable. One focus, circle. Persisting (persist) until imaging end or disappearing before (disappear); % relative to all foci.

Fig. 2

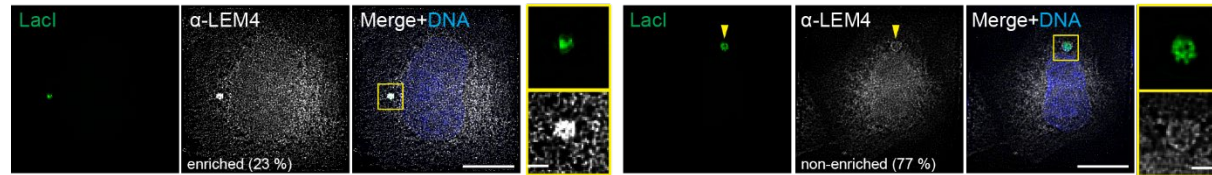
A



B



C

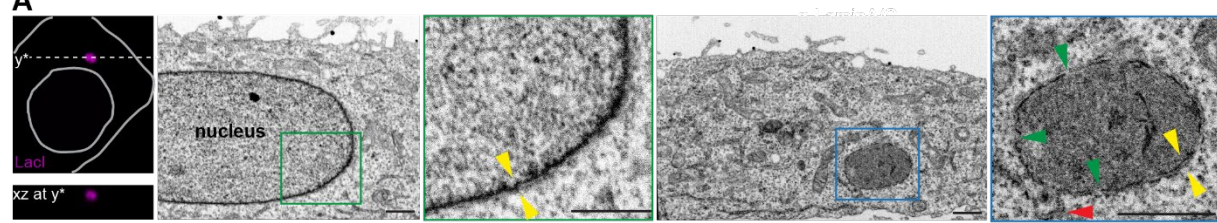


ER enwraps cytoplasmic plasmid DNA.

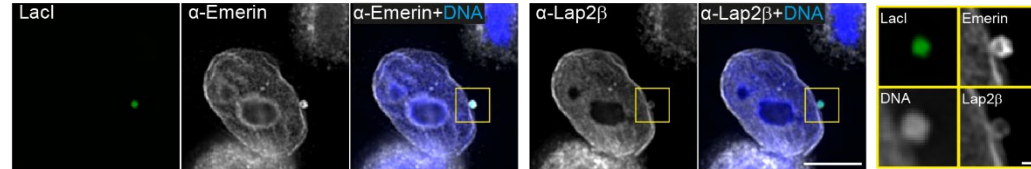
(A-C) Representative images of the localization of ER reporters in pLacO transfected HeLa-LacI cells 24 hours after lipofection with the frequency of two localization patterns (enriched and non-enriched, relative to the intensity of the surrounding ER). DNA, blue (Hoechst stain). Single z-slice images, deconvolved. Insets: focus; scale bars: in big images: 10 μ m, in insets: 1 μ m. **(A)** Transient expression of Sec61-mCherry. Pooled data of 4 exp., total n(cells): 76. n(foci): 79. % relative to all foci analyzed. **(B)** Transient expression of GFP-KDEL. Arrowhead, position of focus; 3 exp.; total n(cells): 80; n(foci): 96. % relative to all foci analyzed. **(C)** Anti-LEM4 immunostaining 24 hours after pLacO lipofection. 2 exp. n(cells): 84; n(foci): 84. % relative to all foci analyzed.

Fig. 3

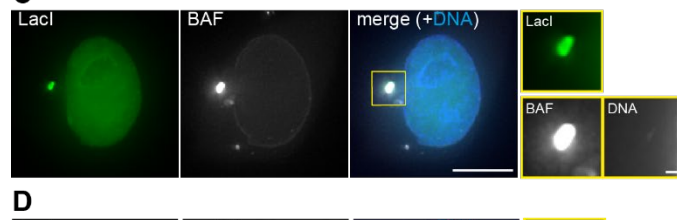
A



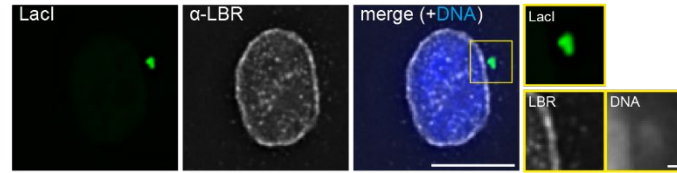
B



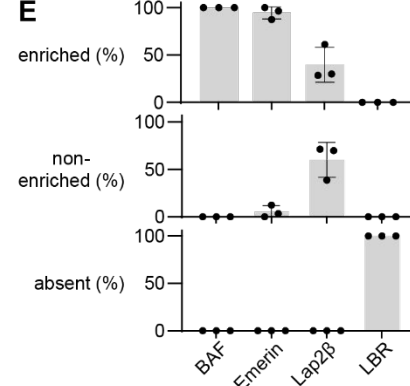
C



D



E

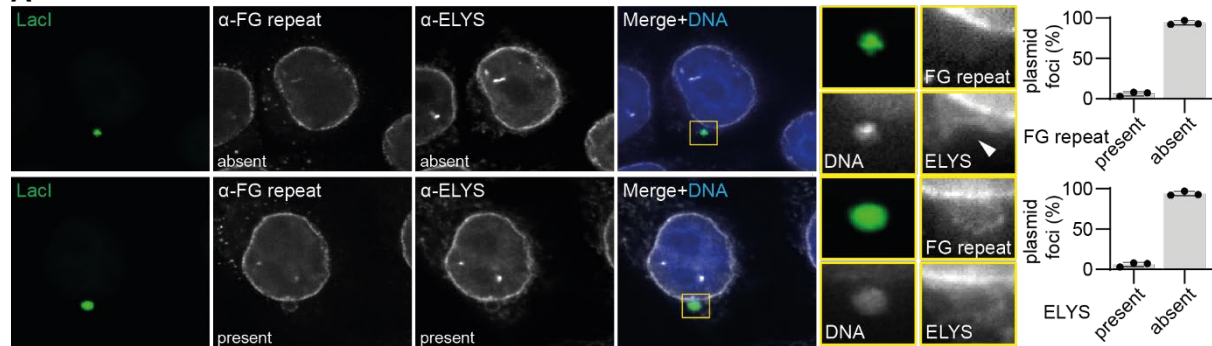


A special double membrane enwraps cytoplasmic plasmid DNA.

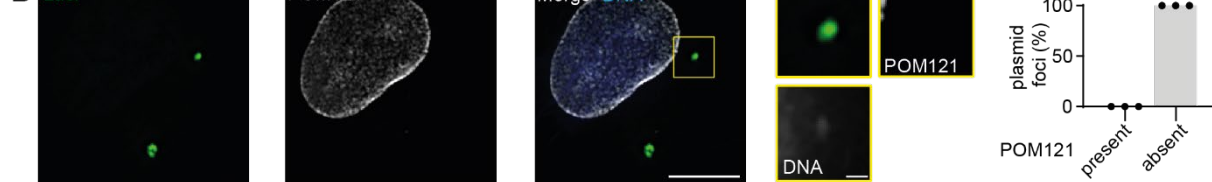
(A) Correlative fluorescence with electron microscopy (CLEM) of an interphase cell containing one pLacO focus. Left images: confocal images; upper: single z-slice xy-image superimposed with a grey cell outline and the y*-cut line; lower: xz-view of the upper cell along the dashed y* line. The first overview EM image depicts a part of the nucleus of the cell shown in the confocal images. The second overview EM image corresponds to the same cell imaged at y*. Insets: focus, blue square; part of the interphase nucleus, green square; double-layered NE, yellow arrowhead pair; membrane connecting proximal ER and the focus, red arrowhead; gaps in the focus envelope, green arrowheads; scale bars 1 μ m. **(B-D)** Representative images of the localization of indicated reporters and foci in HeLa-Lacl. Images: single z-slice, deconvolved; insets: foci; scale bars: in big images 10 μ m; in insets: 1 μ m; DNA, blue (Hoechst stain). **(E)** Quantification of relative localization patterns (absent, non-enriched, enriched relative to the NE) of indicated reporters 24 hours after lipofection of pLacO. 3 exp. (circles); mean and SD, each with total numbers: n(Lap2β, foci): 52; n(Emerin, foci): 62; n(LBR, foci): 63; n(LBR, cells): 54; n(BAF, foci): 23; n(BAF, cells): 23.

Fig. 4

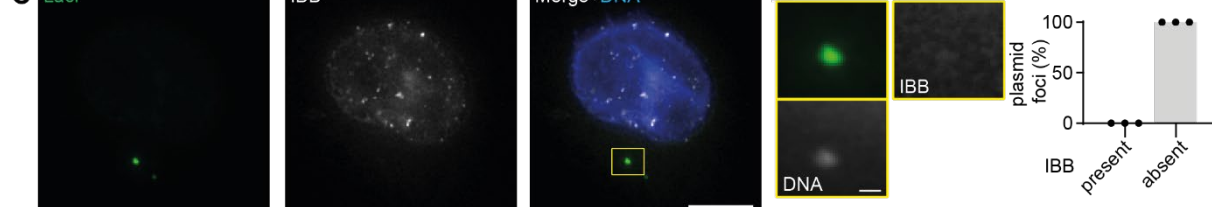
A



B



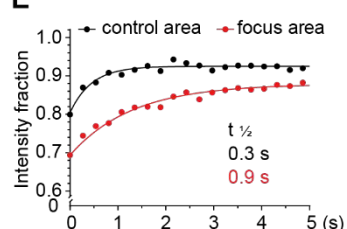
C



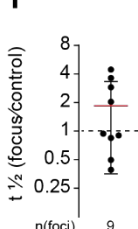
D



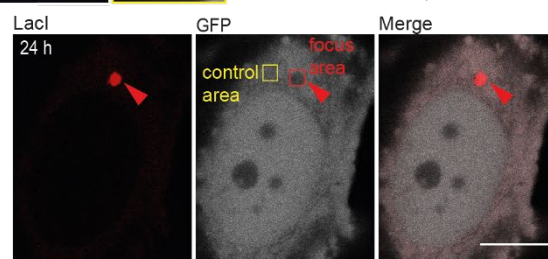
E



F



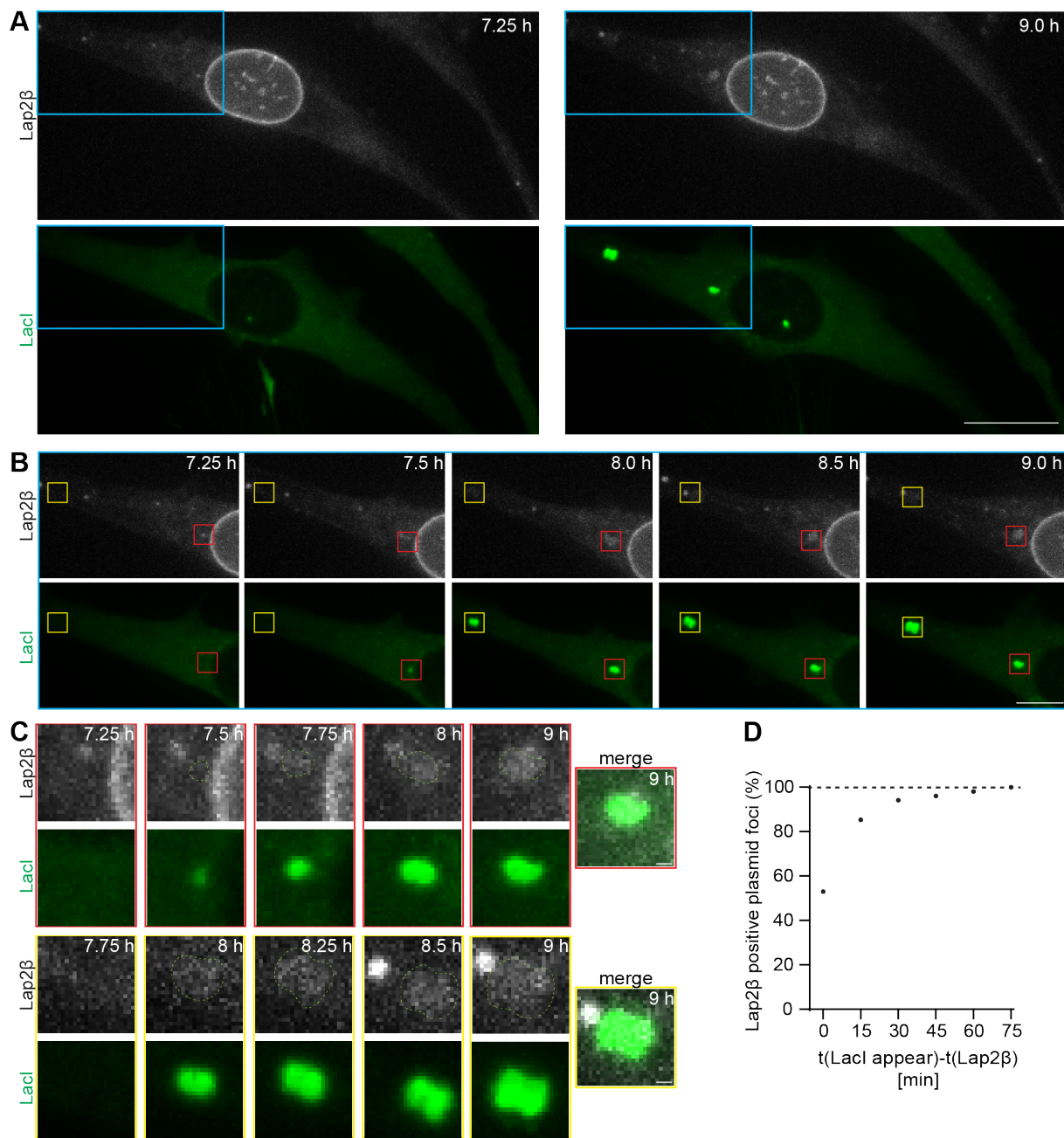
G



The plasmid enwrapping envelope is devoid of functional NPCs but not closed.

(A-D) Representative images of HeLa-Lacl cells 24 hours after lipofection with pLacO. Insets: focus; scale bars: in big images: 10 μ m, in insets: 1 μ m; focus, arrowheads. DNA, blue (Hoechst stain). Right quantification; % relative to all foci; 2-3 exp., 1 exp., circle; mean & SD. **(A)** Immunostaining for ELYS and FG-repeats. Upper: absence, lower: presence example, 3 exp., n(ELYS, FG-repeats, foci): 111. **(B-D)** Images single z-slice, deconvolved. **(B)** POM121. 3 exp.; n(foci): 55. **(C)** IBB. 3 exp.; n(foci): 22; n(cells): 17. **(D)** RCC1. 2 exp.; n(foci): 55; n(RCC1, cells): 48. **(E-G)** FRAP analysis in HeLa cells transiently expressing LacI-mCherry and soluble GFP 24 hours after pLacO transfection. **(E)** Recovery of bleached GFP over time; $t_{1/2}$: recovery time for half of GFP intensity. **(F)** Quantification of (E): Ratio of $t_{1/2}$ at focus area versus control area. Mean & SD; 3 exp.; 1 measurement, circle. n(foci): 9. **(G)** Representative images of bleaching areas. Focus area, red square; control area, yellow area. Scale bar: 10 μ m.

Fig. 5



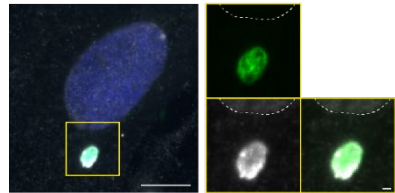
A plasmid focus formed in the cytoplasm is rapidly enwrapped by membrane.

(A-C) Time-lapse images of HeLa cells stably expressing Lap2 β -GFP (Lap2 β) and transiently expressing LacI-mCherry (LacI) after lipofection with pLacO. Time, after pLacO transfection. **(A)** Overview images of the cell at 7.25 hours and 9 hours after transfection. The area in the blue square is enlarged in **(B)**. Scale bar, 20 μ m. **(B)** Enlarged part of the cell in **(A)**. Focus forms with concomitant Lap2 β association, red square. Focus forms with no observable Lap2 β association during imaging, yellow square; scale bar, 10 μ m. **(C)** Enlarged squares of **(B)**. Focus outline, superimposed dashed line; lower row: Lap2 β channel boosted, non-boosted images in **(A,B)**; scale bar, 1 μ m. **(D)** Cumulative fraction of foci associated with Lap2 β in dependence on the duration of Lap2 β association after focus appearance. 1 exp., n(foci): 105; n(cells): 49.

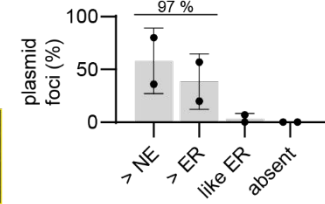
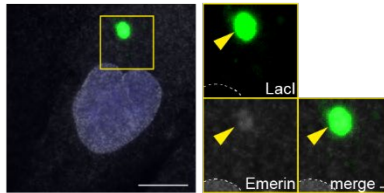
Fig. 6

A

Emerin > NE

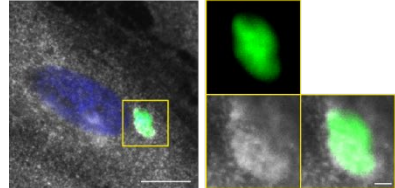


Emerin > ER

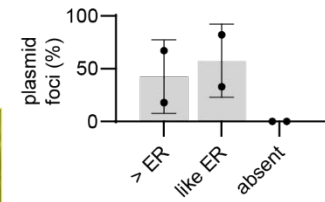
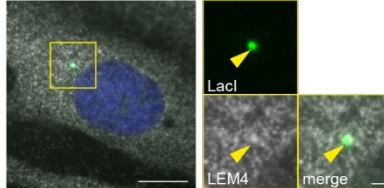


B

LEM4 > ER



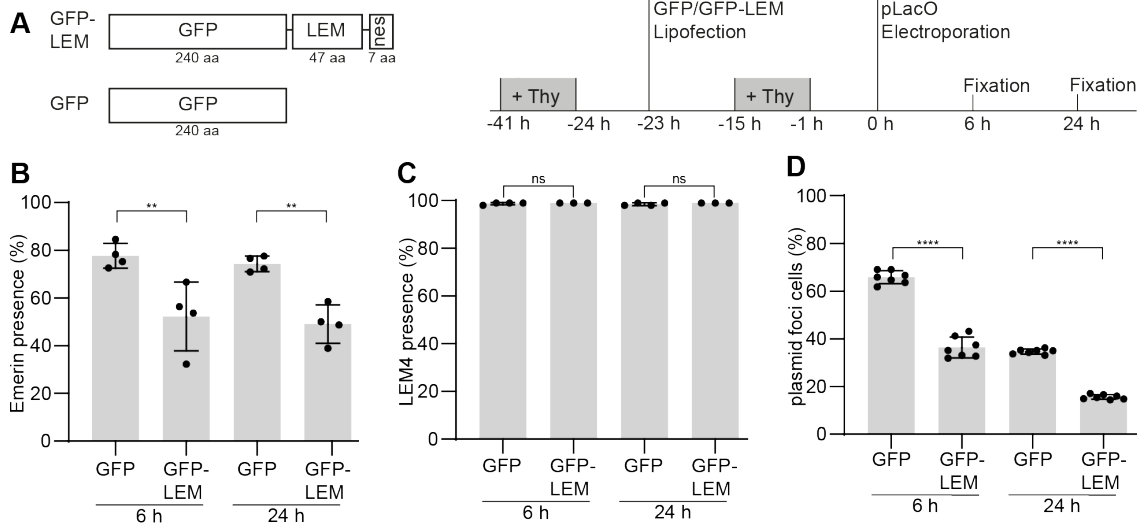
LEM4 like ER



Exclusomes containing plasmid DNA exist in primary human fibroblasts.

(A, B) Primary human fibroblasts 48 hours after lipofection with pLacO and plasmid encoding LacI-NLS-GFP, immunostained for Emerin (A) and LEM4 (B). Single z-slice images. Insets: focus; scale bars: in big images 10 μ m; in insets: 1 μ m; DNA, blue (Hoechst stain). **(A)** Representative images of indicated classification. Outline of nucleus, dashed line. Right graph: Emerin's intensity relative to the NE (> NE) and the ER (> ER, like ER) in cells with 1 cytoplasmic focus. 2 exp., 1 exp., circle; mean and SD; n(foci): 29. **(B)** Representative images for indicated classification of LEM4. Right graph: LEM4 intensity at focus relative to the ER (> ER, like ER) in cells with 1 cytoplasmic focus. 2 exp., 1 exp., circle; mean and SD; n(foci): 38.

Fig. 7

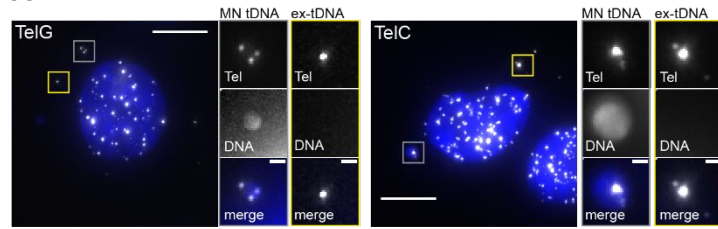


Overexpression of Emerin's LEM domain reduces cells with plasmid foci.

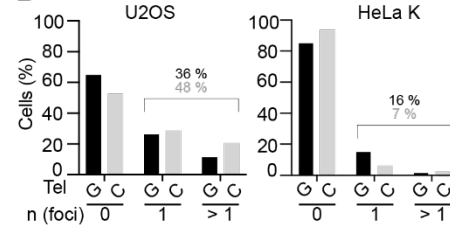
(A) Scheme of fusion proteins transiently overexpressed in HeLa-LacI cells (left side) and experimental procedure (right side). GFP-LEM-nes (“GFP-LEM”), soluble GFP (“GFP”); aa: amino acid residues. + Thy: thymidine treatment; time, relative to pLacO transfection. **(B)** Presence of Emerin at cytoplasmic foci 6 hours and 24 hours after electroporation of pLacO. 4 exp., 1 exp., circle; mean and SD; two-way Anova, **: p <0.01; n(foci): GFP 6 hours: 589; GFP 24 hours: 458; GFP-LEM 6 hours: 474; GFP-LEM 24 hours: 413. **(C)** Presence of LEM4 at cytoplasmic foci 6 hours and 24 hours after electroporation of pLacO. 3 to 5 exp. 1 exp., circle; mean and SD; two-way Anova; n.s.: not significant; n(foci): GFP 6 hours: 727; GFP 24 hours: 536; GFP-LEM 6 hours: 334; GFP-LEM 24 hours: 280. **(D)** Frequency of cells containing at least one cytoplasmic focus in GFP and GFP-LEM expressing cells 6 hours and 24 hours after electroporation. 7 exp., 1 exp., circle; mean and SD; two-way Anova; **** p<0.0001; n(cells): GFP 6 hours: 1428; GFP 24 hours: 1460; GFP-LEM 6 hours: 1471; GFP-LEM 24 hours: 1469.

Fig. 8

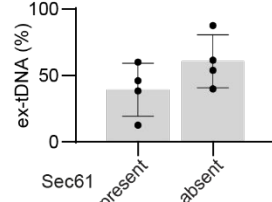
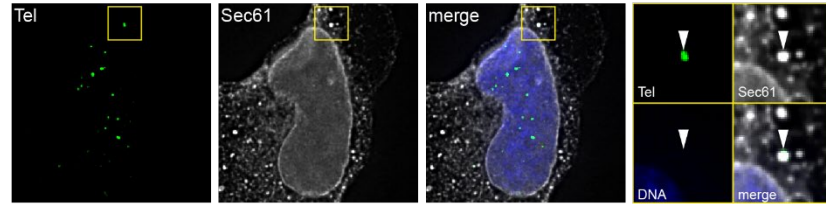
A



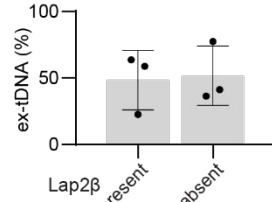
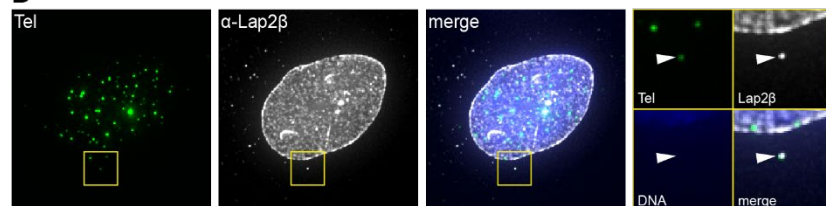
B



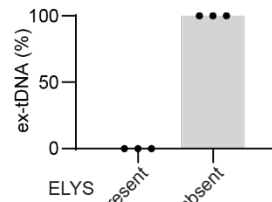
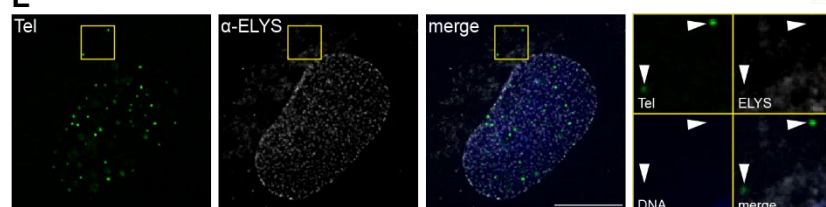
C



D



E

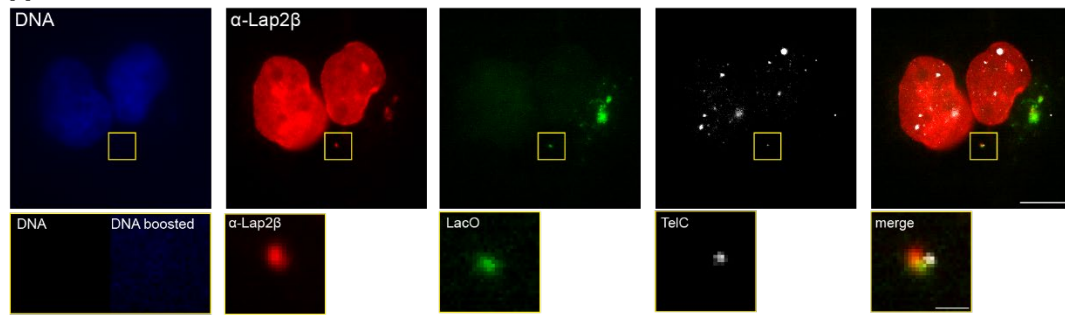


A special envelope enwraps also cytoplasmic extra-chromosomal telomeric DNA.

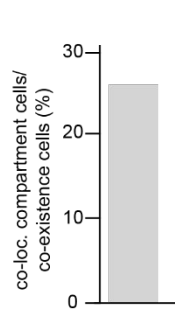
(A) Representative images of U2OS cells FISH stained with TelG and TelC probes. Images max. projected, insets: area with ex-tDNA, yellow squares; area with MN tDNA, gray squares. Scale bars: in big images: 10 μ m; in insets: 1 μ m. DNA, blue (Hoechst stain). **(B)** Frequency of HeLa K and U2OS cells with none, one (1), or more than one (>1) ex-tDNA focus relative to the total cells analyzed. Pooled data of FISH experiments. U2OS-TelG probe: 3 exp.; > 47 cells per exp., total n(cells): 217; U2OS-TelC probe: 3 exp.; > 49 cells per exp., total n(cells): 171; HeLa-TelG probe: 3 exp.; > 55 cells per exp., total n(cells): 210; HeLa-TelC probe: 3 exp.; > 63 cells per exp., total n(cells): 209. **(C-E)** Representative single z-slice images of FISH-IF stained U2OS cells depicting the localization of the reporter proteins (left); quantification of colocalization of respective marker at ex-tDNA focus (right, plot). Big images: max. projected deconvolved; arrowheads, ex-tDNA foci ; Areas of tDNA foci, insets. Scale bars: big images: 10 μ m, insets: 1 μ m; 3 exp.; DNA, blue (Hoechst stain). Signals of TelG probe, overexpressed of Sec61-mCherry (C) and indicated antibodies (D,E). % relative to all ex-tDNA foci analyzed. Mean & SD. Sec61, 4 exp., 1 exp., circle, n(Sec61, ex-tDNA): 95; Lap2 β , 3 exp. 1 exp., circle, n(Lap2 β , ex-tDNA): 1 54; ELYS, 3 exp. 1 exp., circle, n(ELYS, ex-tDNA): 66.

Fig. 9

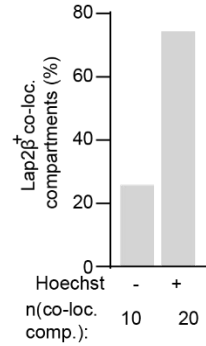
A



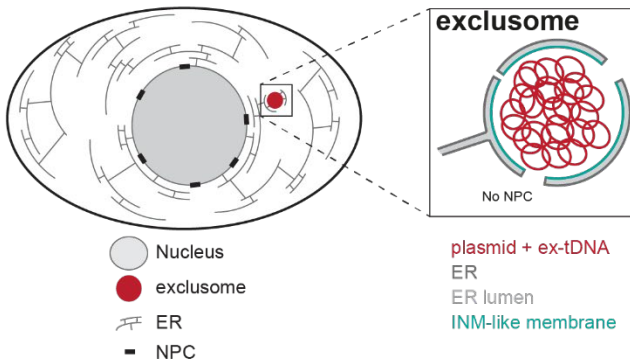
B



C



D

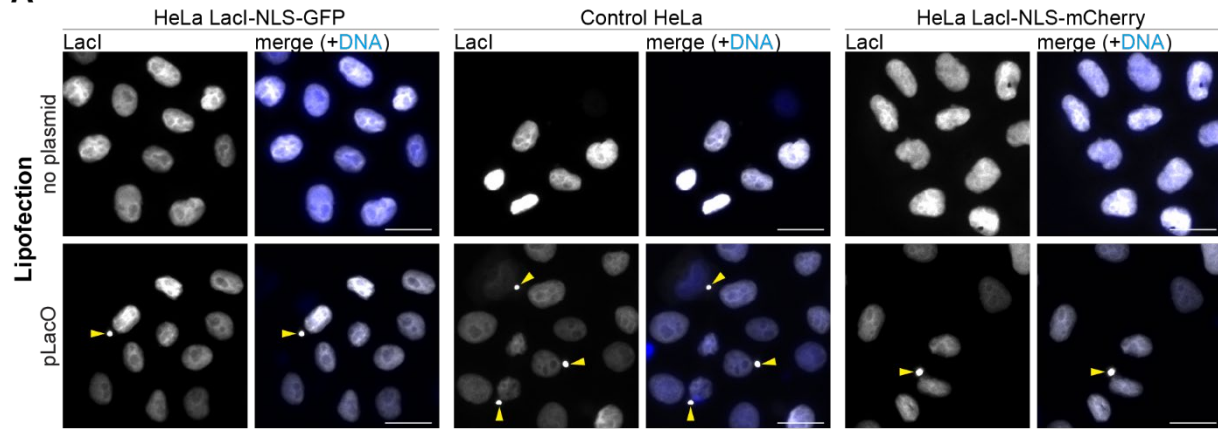


Plasmid DNA and ex-tDNA can be clustered in one exclusome.

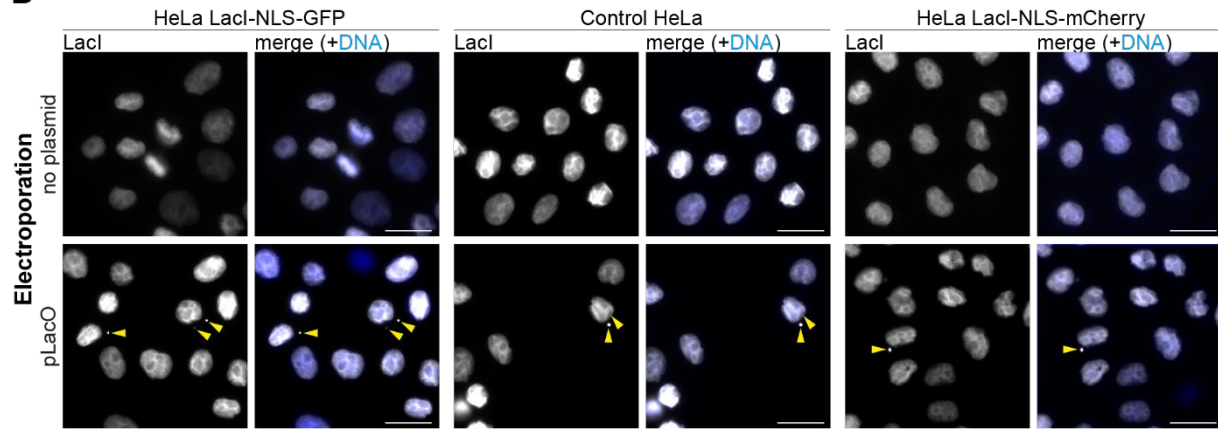
(A) Representative image of a U2OS cell transfected with pLacO, fixed, hybridized with TelC and LacO probes and immunostained against Lap2β. DNA, blue (Hoechst stain). Inset: cytoplasmic compartment with two DNA species; DNA stain inset boosted, DNA boosted. Scale bars: in big images: 10 μ m, in insets: 1 μ m. **(B)** Frequency of U2OS cells with minimally one co-localization compartment in cells, which contain both DNA species (co-existence cells) 24 hours after pLacO transfection. Pooled data of 3 exp., individual exp. in SFig. 8G. >15 co-localization compartments/exp.; total n(co-existence cells): 155; >3 co-existence cells/exp; total n(co-existence cells): 40. **(C)** Frequency of Lap2β positive cytoplasmic co-localizing compartments. 24 hours after pLacO transfection. Pooled data of 3 exp.; individual exp. in SFig. 8H. >3 co-localizing compartment/exp., total: n(Lap2β+ co-localizing compartment): 30. **(D)** Model of an exclusome in an interphase cell. Overview of a cell with nucleus, ER and exclusome (inlet: the magnified exclusome with details).

SFig. 1

A



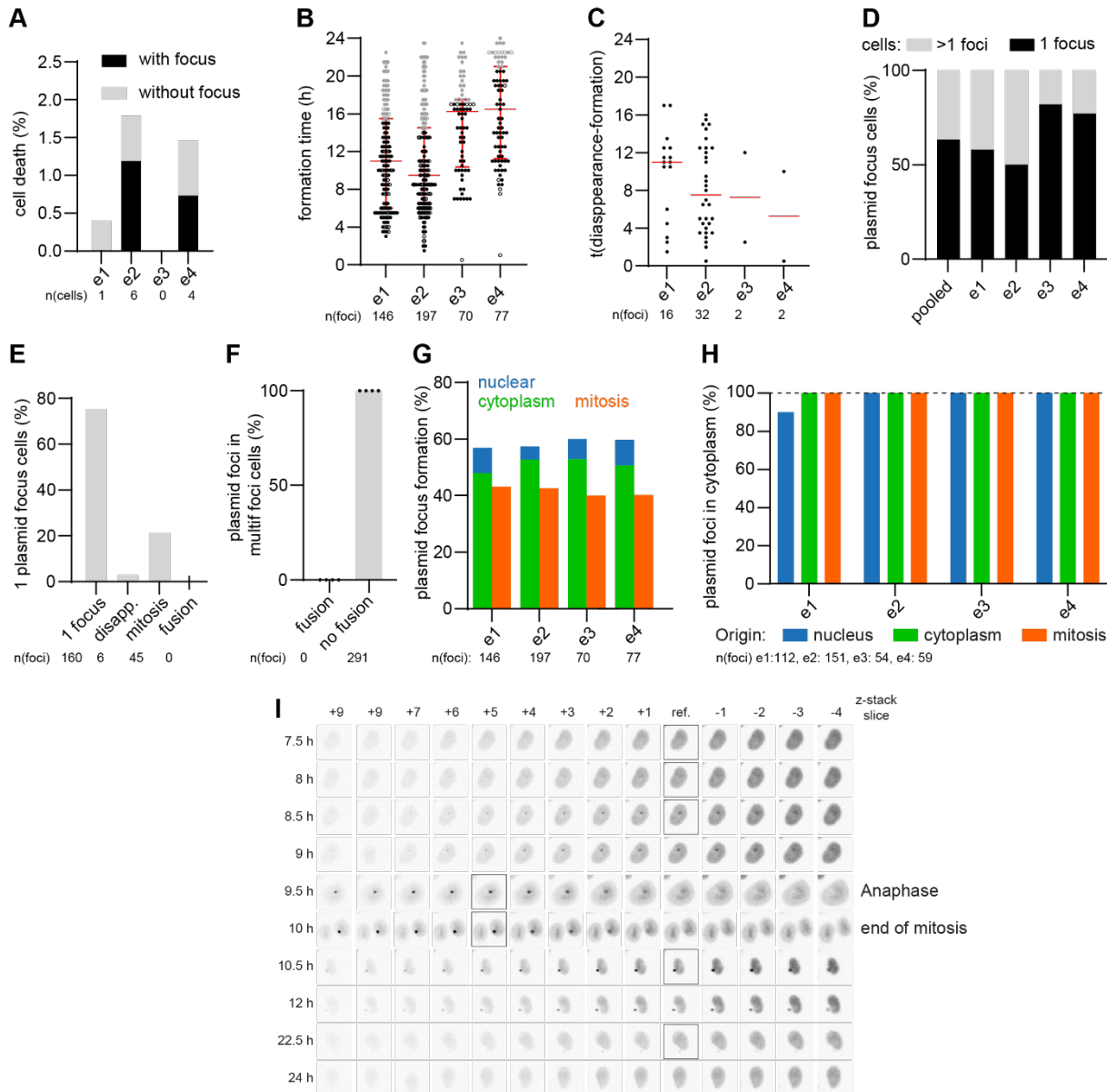
B



Only plasmid-transfected cells have cytoplasmic LacI foci.

(A, B) Images of HeLa-Lacl cells stably expressing LacI-NLS-GFP or LacI-NLS-mCherry lipofected **(A)** or electroporated **(B)** without or with pLacO and fixed 24 hours after transfection. Scale bar, 20 μ m. DNA, blue (Hoechst stain). Plasmid foci in the cytoplasm, yellow arrowheads.

SFig. 2

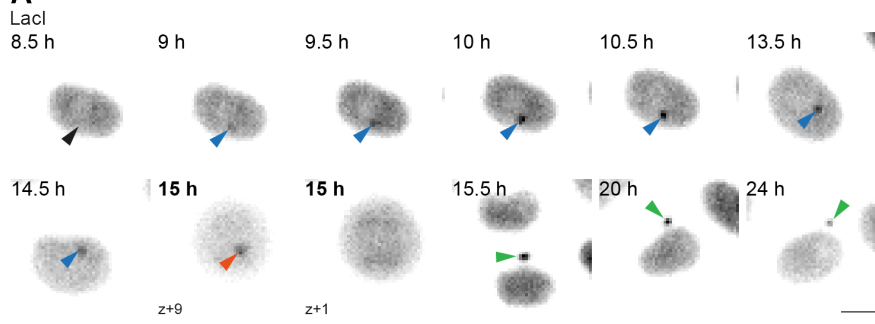


Dynamics of plasmid foci in individual live cell imaging experiments.

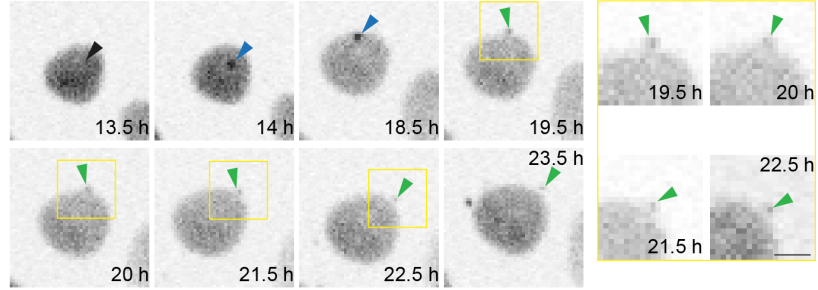
Individual exp., e1 - e4. **(A)** Cell death events until end of imaging. Cells died without focus, grey; died with focus, black; % relative to cells at end. n(cells): 253, 336, 270, 273. **(B)** Timing of focus formation. 1 focus, circle; time, after lipofection; median & interquartile range, red; last 25 % formations, grey. **(C)** Presence period of disappearing foci. 1 focus, circle; median, red line. **(D)** Cumulative frequency of 1-focus cells (black) and multi-foci cells (grey) during imaging period. Maximal number of foci per cell during lifetime of single cells; pooled data, pooled. **(E)** Analysis of origin of 1-focus cells at imaging end. Cell formed 1 focus or divided propagating it, 1 focus; cell formed multiple foci and all but one disappeared, disappeared; partitioning in mitosis resulted in 1-focus cell(s), mitosis; foci fused, fusion. Pooled data. n(1-focus cells): 211. **(F)** Fusion of foci in multi-foci cells. Pooled data. **(G)** Origin of forming foci. Normalized to all foci formed per exp. **(H)** Cytoplasmic foci depending on origin. Last 25 % formations excluded. n(foci): 112; 100 % reference, dashed line. **(I)** Focus formation in the nucleoplasm. Cell as Fig. 1A (nucleoplasmic formation, corresponding images with black squares) with z-slices above and below reference slice (ref.) Scale bar, 10 μ m. Time, after lipofection. Black horizontal lines, skipped time points.

SFig. 3

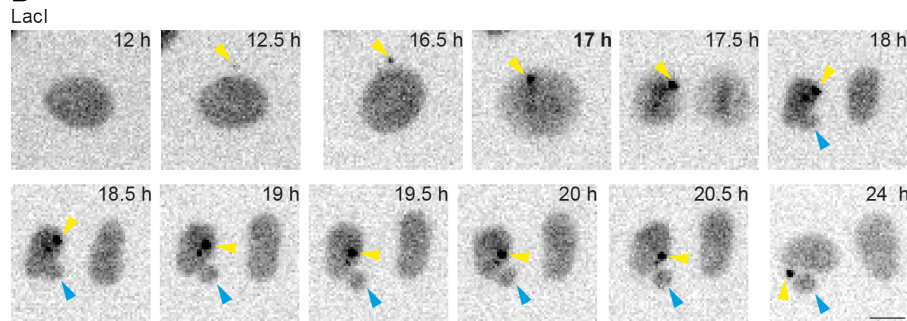
A



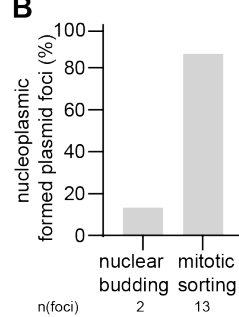
LacI



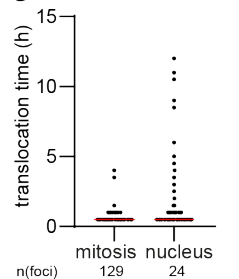
D



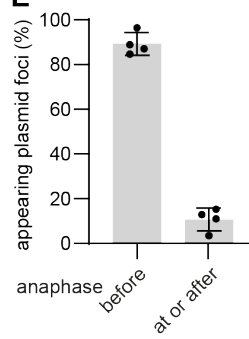
B



C



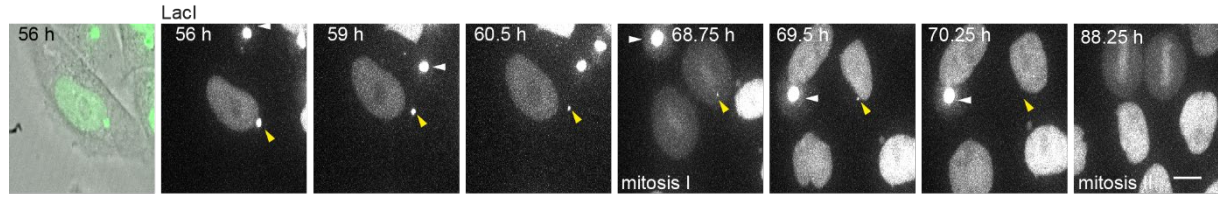
E



How plasmid DNA leaves the nucleus.

(A) Two example time-lapse images of focus formations in HeLa-LacI cells; mitotic sorting (upper) and nuclear budding (lower). Scale bar, 10 μ m. Time, after lipofection; bold time, mitosis. Arrowheads: nucleoplasmic, blue; cytoplasmic, green; mitosis, orange; future focus formation area, black; single z-slices. **(B)** Quantification of events shown in **(A)**. Pooled data of 4 exp.; only foci analyzed, which appeared in the nucleoplasm but not at the border of the nuclear LacI-NLS-GFP fluorescence neither on nucleoplasmic side (see method); n(foci): 15. **(C)** Duration between the first detection of a focus and its first localization in the cytoplasm. Only plasmid foci formed either during mitosis or in the nucleus, appearing during the first 75 % of the formation time of all plasmid foci formations and translocating into the cytoplasm, were analyzed. 1 plasmid focus, circle; pooled data of 4 exp.; median, red line; n(foci): 24. **(D)** Time-lapse images contrasting focus (yellow arrowhead) and mitotic micronucleus formations (light blue arrowhead) in HeLa-LacI cells. Scale bar, 10 μ m. Time, after lipofection. **(E)** Plasmid foci formed during mitosis relative to anaphase. 4 exp. (circles); mean & SD; n(foci): 207.

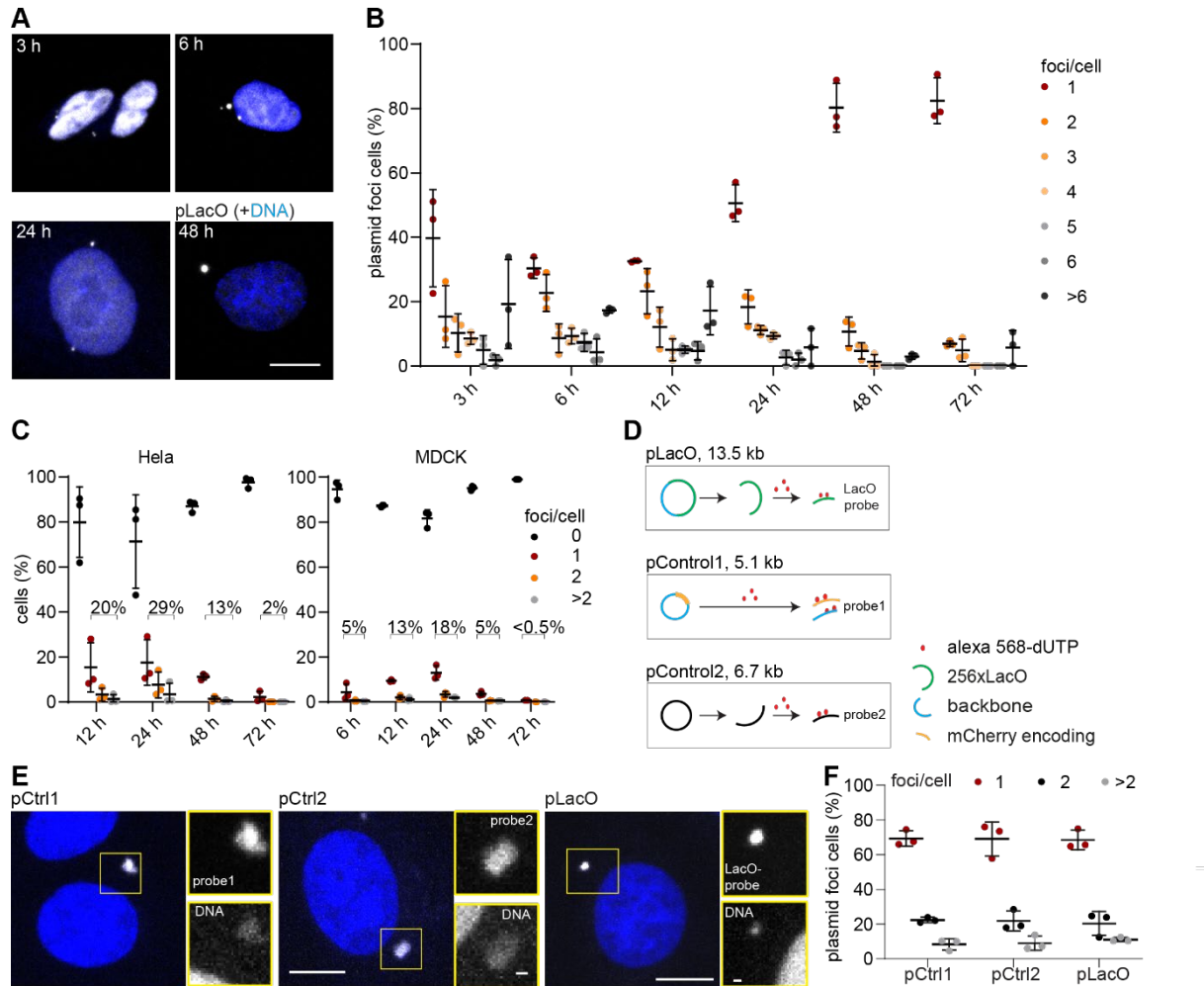
SFig. 4



Fluorescence dynamics of plasmid foci in long-term movies.

Representative time-lapse images of HeLa-Lacl cells showing the disappearance of a focus between 56 hours and 88.25 hours after transfection. Plasmid focus, yellow arrowheads. Persistent brightness of a focus (white arrowhead) in a neighboring cell shows that the disappearance of fluorescence at a focus is not because of bleaching. Cell outline is shown by transmission light in the first frame (56 hours). Scale bar, 10 μ m.

SFig. 5

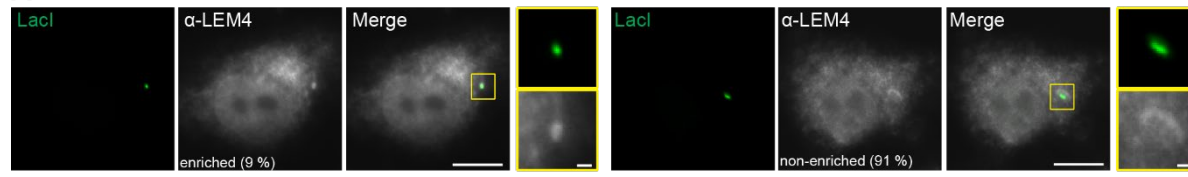


Time, transfection method, and plasmid type dependent reaction towards transfected plasmid DNA.

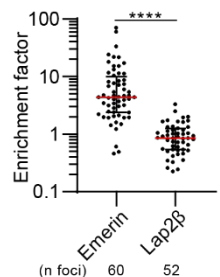
(A, B) MDCK-Lacl cells electroporated with pLacO fixed, imaged, and analyzed at indicated times after electroporation. **(A)** Example images. Scale bar, 10 μ m. **(B)** 7 classes (1 - >6) of plasmid foci per cell. 3 exp. 1 exp, circle. Mean & SD; n(cells, 3 hours): 166, n(cells, 6 hours): 162, n(cells, 12 hours): 175, n(cells, 24 hours): 161, n(cells, 48 hours): 167, n(cells, 72 hours): 115. **(C)** 4 classes (0 - >2) of plasmid foci per HeLa-Lacl (left panel) and MDCK-Lacl (right panel) cell at indicated times after lipofection. 3 exp. 1 exp., circle; Mean & SD. HeLa-Lacl: n(cells, 12 hours): 1092; n(cells, 24 hours): 778; n(cells, 48 hours): 1442; n(cells, 72 hours): 7164. MDCK-Lacl: n(cells, 6 hours): 3134; n(cells, 12 hours): 1367; n(cells, 24 hours): 1099; n(cells, 48 hours): 4176; n(cells, 72 hours): 17476. **(D)** Scheme illustrating three transfected plasmids and corresponding FISH probes used in (E, F). **(E)** Representative images of FISH on HeLa-Lacl cells lipofected with either pLacO (LacO probe), pControl1 (pCtrl1, probe1), or pControl2 (pCtrl2, probe2) 24 hours after transfection. Images are max. intensity-projected z-stacks. Insets: plasmid foci; scale bars: big images: 10 μ m; insets, 1 μ m. **(F)** 3 classes (1 - >2) of plasmid foci per HeLa-Lacl cell depending on the transfected plasmid. 3 exp, n>50 per exp.

SFig. 6

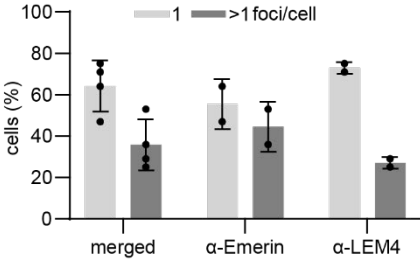
A



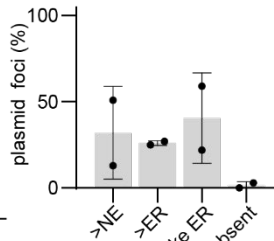
B



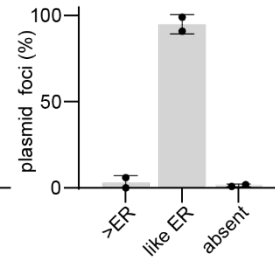
C



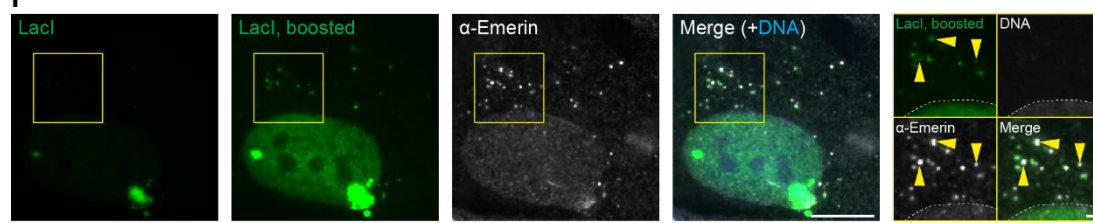
D



E



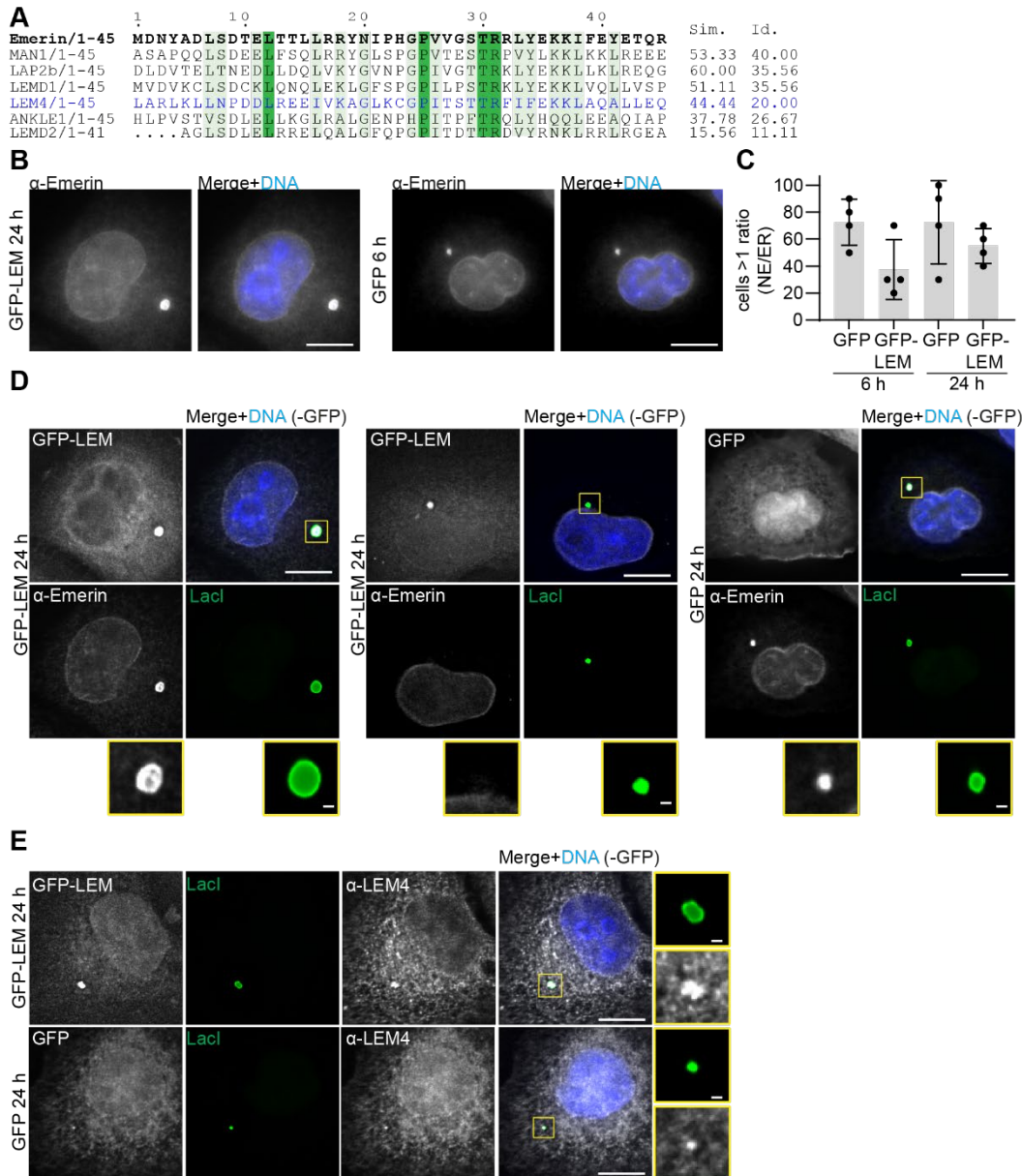
F



Detailed characterization of the exclusome.

(A) HeLa-Lacl cells electroporated with pLacO and 24 hours later immunostained for LEM4. Single z-slice images; insets: plasmid foci; scale bars: big images, 10 μ m; insets, 1 μ m. Pooled data of 2 exp.; n(cells): 124. **(B)** A ratio-based fluorescence enrichment analysis for Emerin and Lap2 β at plasmid foci in HeLa-Lacl cells, 24 hours after pLacO transfection. 3 exp. pooled; plasmid focus, circle. Non-paired t-test with log (value); ****: p<0.0001. **(C-F)** Primary human fibroblasts 48 hours after co-lipofection with pLacO and plasmid encoding Lacl-NLS-GFP. **(C)** Frequency of 1-focus cells and multi-focus cells. 4 exp. 1 exp, circle; n(cells): 106; mean & SD. **(D, E)** Enrichment classes relative to the NE and the ER based on measured intensities for Emerin **(D)** and LEM4 **(E)** in multi-foci cells. 2 exp., 1 exp., circle; mean & SD; n(Emerin, foci): 227; n(Emerin, cells): 54; n(LEM4, foci): 158; n(LEM4, cells): 52. **(F)** Example image of primary human fibroblast 48 hours after transfection and immunostained for Emerin. Single z-slice images. Insets: several plasmid foci; scale bars: in big images 10 μ m; in insets: 1 μ m; DNA in overview, blue; inset, gray (Hoechst stain). Plasmid foci enriched for Emerin compared to nuclear envelope of same cell, yellow arrowheads. Nucleus outline, dashed line.

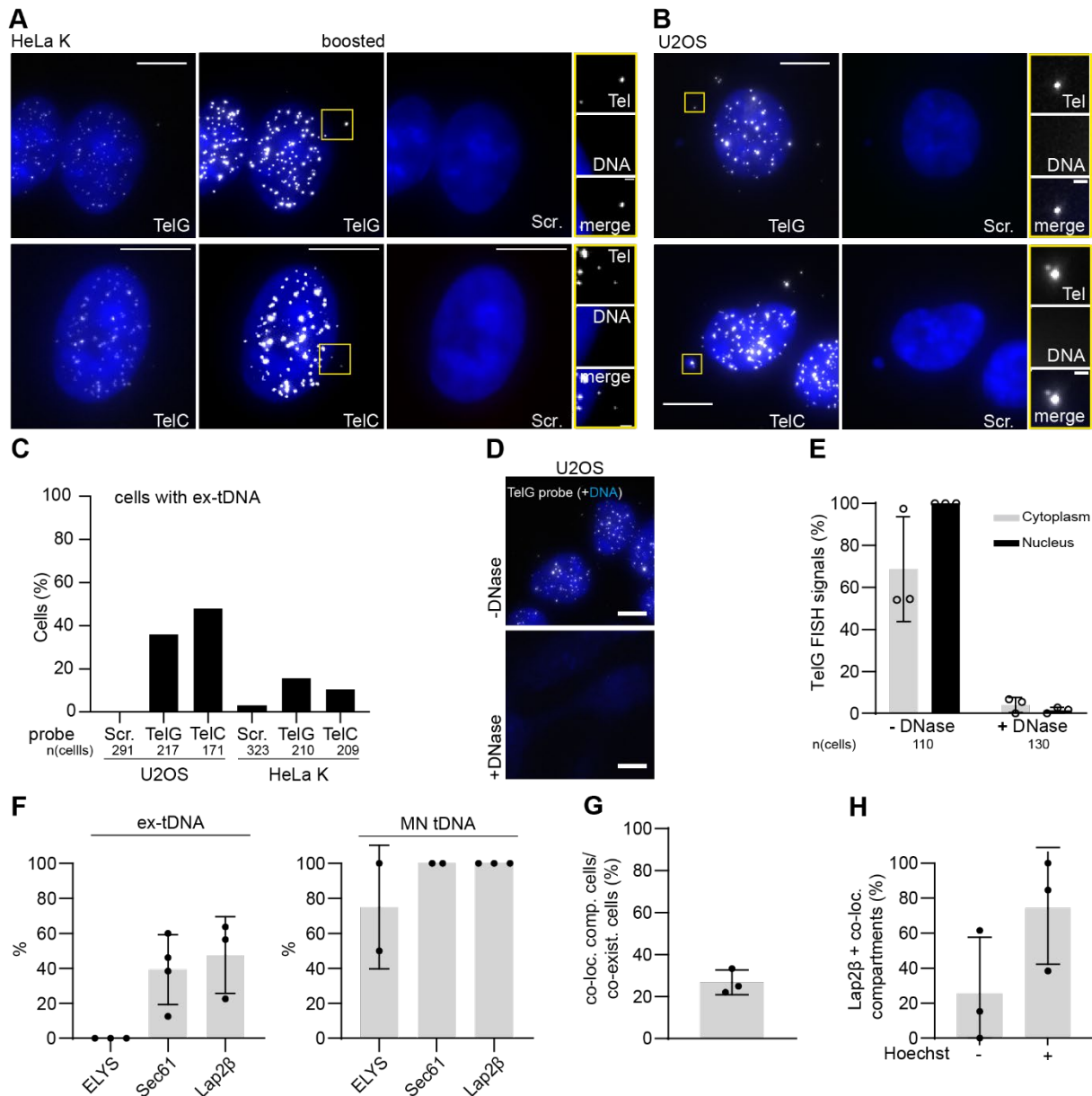
SFig. 7



Effects of overexpression of Emerin's LEM domain.

(A) Amino-acid alignment for the LEM-domain of various human LEM-domain proteins. Percentage of similar (Sim.) and identical (Id.) residues compared to Emerin (bold). LEM-domain of LEM4, blue. Sim. residues, light green; Id. residues, dark green. **(B-E)** HeLa-Lacl cells transiently expressing GFP-LEM or GFP 6 hours **(C)** and 24 hours **(B-E)** after electroporation with pLacO. DNA, blue (Hoechst staining). **(B)** Boosted single z-slice images to visualize ER. Same cells as in **(D)** (left & right panel) immunostained for Emerin. Scale bar, 10 μ m. **(C)** Cells, with a higher measured intensity of Emerin at the NE compared to the ER. 4 exp. 1 exp. circle; mean & SD. **(D, E)** Deconvolved single z-slice images to visualize plasmid foci. Cells were immunostained for Emerin **(D)** or LEM4 **(E)**. Insets: plasmid focus. Scale bar: in big images, 10 μ m; insets, 1 μ m.

SFig. 8



Interphase U2OS and HeLa K cells with ex-tDNA.

(A, B) Representative max. projected images of HeLa K (**A**) and U2OS (**B**) cells with either TelG or TelC probes plus scramble probes (scr.). Insets: ex-tDNA foci. Imaging conditions of (**A**) and (**B**) were the same; corresponding display; except for when FISH signals were boosted (boosted). Scale bar, 10 μ m. **(C)** Percentages of HeLa K, U2OS cells containing ex-tDNA. Pooled data of 3 to 5 exp. U2OS with TelG: 3 exp; n(cells): 47, 73, 97; U2OS with TelC: 3 exp; n(cells): 57, 49, 65; U2OS with scr.: 5 exp; n(cells): 57, 49, 65, 73, 47. HeLa with TelG: 3 exp; n(cells): 55, 59, 96; HeLa-TelC: 3 exp; n(cells): 82, 64, 63; HeLa with scr.: 5 exp; n(cells): 82, 64, 63, 55, 59. **(D, E)** Representative max. projected images (**D**) and quantification of U2OS (**E**) with nuclear and cytoplasmic TelG FISH signals, with and without DNase I treatment. DNA, blue (Hoechst stain). Scale bar, 10 μ m; mean & SD; 3 exp. (circles). **(F)** Colocalization of indicated proteins with ex-tDNA (left side) and MN tDNA (right side). 3 exp. (circles); mean & SD; foci: n(Lap2 β , ex-tDNA): 154; n(Lap2 β , MN tDNA): 12; n(Sec61, ex-tDNA): 95; n(Sec61, MN tDNA): 6; n(ELYS, ex-tDNA): 66; n(ELYS, MN tDNA): 6. **(G)** U2OS cells with minimally one co-localization (co-loc.) compartment (comp.) in cells, which contain both ex-tDNA and plasmid DNA (termed co-existence cells (co-exist.)) 24 hours after pLacO transfection. 1 exp,

circle; n(co-exist. cells): 155; n(co-loc comp): 46; mean & SD. (H) Quantification of Hoechst signal at Lap2 β^+ co-localization (co-loc.) compartments 24 hours after pLacO transfection. 3 exp. (circles); n(co-existence cells): 46; n(Lap2 β^+ co-localization compartments): 30; mean & SD.